Homogenized rigid-plastic model for masonry walls subjected to impact

Gabriele Milani[1], Paulo B. Lourenço[2], Antonio Tralli[3]

(1) Corresponding Author. Department of Structural Engineering (DIS), Technical University (Politecnico) of Milan, Piazza Leonardo da Vinci 32, 20133 Milan, Italy (e-mail: milani@stru.polimi.it).

(2) ISISE, Department of Civil Engineering, School of Engineering, University of Minho, Campus de Azurém, 4800-058 Guimarães, Portugal.

(3) Department of Engineering, University of Ferrara, Via Saragat 1, 44100 Ferrara, Italy.

Abstract

A simple rigid-plastic homogenization model for the analysis of masonry structures subjected to out-of-plane impact loads is presented. The objective is to propose a model characterized by a few material parameters, numerically inexpensive and very stable. Bricks and mortar joints are assumed rigid perfectly plastic and obeying an associated flow rule. In order to take into account the effect of brickwork texture, out-of-plane anisotropic masonry failure surfaces are obtained by means of a limit analysis approach, in which the unit cell is subdivided into a fixed number of sub-domains and layers along the thickness. A polynomial representation of micro-stress tensor components is utilized inside each sub-domain, assuring both stress tensor admissibility on a regular grid of points and continuity of the stress vector at the interfaces between contiguous sub-domains. Limited strength (frictional failure with compressive cap and tension cutoff) of brick-mortar interfaces is also considered in the model, thus allowing the reproduction of elementary cell failures due to the possible insufficient resistance of the bond between units and joints.

Triangular Kirchhoff-Love elements with linear interpolation of the displacement field and constant moment within each element are used at a structural level. In this framework, a simple quadratic programming problem is obtained to analyze entire walls subjected to impacts.

In order to test the capabilities of the approach proposed, two examples of technical interest are discussed, namely a running bond masonry wall constrained at three edges and subjected to a point impact load and a masonry square plate constrained at four edges and subjected to a distributed dynamic pressure simulating an air-blast. Only for the first example, numerical and experimental data are available, whereas for the second example insufficient information is at disposal from the literature. Comparisons with standard elastic-plastic procedures conducted by means of commercial FE codes are also provided. Despite the obvious approximations and limitations connected to the utilization of a rigid-plastic model for masonry, the approach proposed seems able to provide results in agreement with alternative expensive numerical elasto-plastic approaches, but requiring only negligible processing time. Therefore, the proposed simple tool can be used (in addition to more sophisticated but expensive non-linear procedures) by practitioners to have a fast estimation of masonry behavior subjected to impact.

Keywords: Masonry, out-of-plane loads, homogenization, dynamic rigid-plasticity, impact.

1 Introduction

Structures and buildings are occasionally called upon to withstand exceptional dynamic loading regimes, caused by accidental events, such as for instance impacts from vehicles or gas / terrorist explosions. In order to take into account the effect induced on structures by exceptional loads, codes of practice of many countries, e.g. EN 1991-1-7:2006 (2006), require the safety assessment of buildings when subjected to *ad-hoc* equivalent static loads. Such loads are usually obtained through empirical coefficients and are aimed at mimicking the effect of quasi instantaneous dynamic actions.

An alternative approach to the assumption of simplified static load distributions, usually based on simplifications and rules of thumb, is the utilization of finite element non-linear dynamic analyses (see e.g. Burnett et al. 2007 and Wu and Hao 2006 and 2008), almost always performed using commercial software available in the market. According to authors' knowledge, commercial codes devoted exclusively to the non-linear dynamic analysis of brickwork are still lacking. Moreover, when dealing with impact on masonry structures, a non-linear standard dynamic finite element approach is usually only applicable to walls of small dimensions, basically for research purposes and requires considerable expertise. Still, the computational cost is usually prohibitive, due to the need of modeling separately mortar joints and units in the framework of a heterogeneous approach.

Due to the above reasons, despite the importance of the problem and the growing interest in the scientific community related to the safety assessment of structures subjected to quasi instantaneous dynamic loads, only a few works dealing with this subject seem to exist (Mayrhofer 2002, Gilbert et al. 1998 and 2002a, Wu and Hao 2006 and 2008, Wang et al. 2009).

Also, only a few laboratory experimental investigations devoted to the study of dynamic loads simulating vehicles impacts on parapets (Gilbert et al. 1998 and 2002a) and air-blasting, e.g. Mayrhofer 2002 and Astbury et al. 1970, are available. These experimental programs aim at providing simplified assessment formulas and design recommendations.

In this framework, it is appealing to develop a simple FE numerical approach for masonry subjected to low and high velocity impacts that avoids independent modeling of bricks and mortar joints, that requires a very limited number of input parameters to set and that is able to reproduce failure mechanisms and displacements evolution at successive time steps.

As a matter of fact, the response of masonry when loaded out-of-plane is strongly influenced by the anisotropic behavior of brickwork at failure (see, e.g. Gilbert et al. 2002a, Milani et al. 2006a). Furthermore, despite the fact that masonry behavior near failure when loaded out-of-plane is locally brittle, laboratory tests (see e.g. Southcombe et al. 1995) conducted on entire masonry walls in two-

way bending, have shown that failure takes place along a definite pattern of lines, with a relatively ductile response. This inspired the utilization of approximate analytical solutions based both on the yield line theory and on the fracture line theory (Sinha 1978), able to predict with sufficient accuracy the ultimate load bearing capacity of entire walls, see Figure 1. Up to now, the yield line approach seems the most suitable to apply in practice for the evaluation of masonry behavior, a statement corroborated by the adoption of this approach in many codes of practice, as for instance BS 5628 (1985) and EC6 (1995).

In this framework, here, a homogenized rigid-plastic FE approach for dynamic analyses of masonry structures is presented. Bricks and mortar joints are assumed rigid perfectly plastic and obeying an associated flow rule. Out-of-plane anisotropic masonry failure surfaces are obtained by means of a limit analysis approach, in which the unit cell is subdivided into a fixed number of sub-domains and layers along the thickness. A polynomial representation of micro-stress tensor components is utilized inside each sub-domain, assuring stress tensor admissibility on a regular grid of points and continuity of the stress vector at the interfaces between contiguous sub-domains. Limited strength of bricks-mortar interfaces is also considered in the model, given by frictional failure with a compressive cap and tension cutoff, thus making the reproduction of elementary cell failures due to the insufficient resistance of the bond between units and joints possible.

Triangular Kirchhoff-Love elements with linear interpolation of the displacement field and constant moment within each element are used at a structural level (Hellan 1967, Hermann 1967). With the aim of numerically evaluating nodal displacements and internal actions at successive time steps, the simple quadratic programming approach proposed in Capurso (1972a and 1972b) is adopted.

Finally, in order to test the capabilities of the model proposed, two examples are treated, namely a running bond masonry wall constrained at three edges and subjected to a point impact load, and a masonry rectangular plate constrained at four edges and subjected to a distributed dynamic pressure simulating an air-blast. The results of the first example are compared with numerical and experimental data available from Gilbert et al. (1998, 2002a and 2002b) and Burnett et al. (2007), whereas, for the second example, only limited numerical results are available from Wu and Hao (2006 and 2008).

It is stressed that insufficient experimental data are available in the literature concerning masonry out-of-plane loaded subjected to impacts. Gilbert et al. (1998, 2002a and 2002b) papers are probably the only ones available giving a full description of masonry response in terms of time-displacement, deformed shapes at successive iterations, mechanical characterization of the constituent materials, etc. Thus, the model here proposed is validated with standard elastic-plastic procedures conducted by means of commercial FE codes and hand calculations, proposed for

instance in Gilbert et al. (2002b) and essentially based on the assumption of perfect plasticity. Despite the simplifications introduced by a rigid plastic assumption, the approach should be able to give reasonable results, as it is also considered in the masonry codes for out-of-plane design (EN 1991-1-7:2006).

Apart from experimental validation, the homogenization approach here presented may be of interest for practitioners and researchers involved in the analysis of masonry structures subjected to impact, because the computational effort is minimal. Finally, sensitivity analyses conducted with the model proposed (almost impossible to carry on with commercial codes), may represent a further help in the design phase, giving a large set of information on panels behavior at successive iterations.

2 Masonry out-of-plane failure surface

A masonry wall Ω constituted by a periodic arrangement of bricks and mortar with a running bond texture (Figure 2) is considered. As shown by Suquet in a general framework (1983) and in other recent masonry papers (Milani et al. 2006a, 2006b and 2006c and Cecchi and Milani 2008), homogenization techniques combined with limit analysis can be applied for the definition of the out-of-plane brickwork strength domain S^{hom}.

In particular, under the assumption of perfect plasticity and associated flow rule for the constituent materials and in the framework of the lower bound limit analysis theorem, an estimation of S^{hom} can be obtained by means of the following (non-linear) optimization problem (see also Figure 2):

$$S^{\text{hom}} = \left\{ (\mathbf{M}, \mathbf{N}) \,\middle|\, \begin{cases} \mathbf{N} = \dfrac{1}{|Y|} \displaystyle\int_{Y \times h} \boldsymbol{\sigma} \, dV & (a) \\ \mathbf{M} = \dfrac{1}{|Y|} \displaystyle\int_{Y \times h} y_3 \boldsymbol{\sigma} \, dV & (b) \\ div\boldsymbol{\sigma} = \mathbf{0} & (c) \\ [\![\boldsymbol{\sigma}]\!]\mathbf{n}^{\text{int}} = \mathbf{0} & (d) \\ \boldsymbol{\sigma}\mathbf{n} \quad \text{anti-periodic} \quad \text{on} \quad \partial Y_l & (e) \\ \boldsymbol{\sigma}(\mathbf{y}) \in S^m \quad \forall \mathbf{y} \in Y^m \,;\, \boldsymbol{\sigma}(\mathbf{y}) \in S^b \quad \forall \mathbf{y} \in Y^b & (f) \end{cases} \right\}$$ (1)

where:

- $\mathbf{N}$ and $\mathbf{M}$ are the macroscopic in-plane (membrane forces) and out-of-plane (bending moments) tensors;

- $\boldsymbol{\sigma}$ denotes the microscopic stress tensor;

- $\mathbf{n}$ is the outward versor of ∂Y_l surface;

- ∂Y_l is defined in Figure 2;

- $[\![\boldsymbol{\sigma}]\!]$ is the jump of micro-stresses across any discontinuity surface of normal $\mathbf{n}^{\text{int}}$;

- S^m and S^b denote respectively the strength domains of mortar and bricks;

- Y is the cross section of the 3D elementary cell with $y_3 = 0$ (see Figure 2), $|Y|$ is its area, V is the elementary cell, h represents the wall thickness and $y = \begin{pmatrix} y_1 & y_2 & y_3 \end{pmatrix}$.

2.1 The micro-mechanical model proposed

A simple admissible and equilibrated micro-mechanical model for the evaluation of S^{hom} is adopted, following the model originally presented in Milani et al. (2006a and 2006c). The unit cell is subdivided into a fixed number of layers along its thickness, as shown in Figure 3-a. For each layer, out-of-plane components σ_{i3} ($i = 1, 2, 3$) of the micro-stress tensor $\boldsymbol{\sigma}$ are set to zero, so that only in-plane components σ_{ij} ($i, j = 1, 2$) are considered active. Furthermore, σ_{ij} ($i, j = 1, 2$) are kept constant along the Δ_{i_L} thickness of each layer, i.e. in each layer $\sigma_{ij} = \sigma_{ij}(y_1, y_2)$. For each layer one-fourth of the REV is sub-divided into nine geometrical elementary entities (*sub-domains*), so that the entire cell is sub-divided into 36 sub-domains (Figure 3-b).

For each sub-domain (k) and layer (i_L), simple polynomial distributions of degree *(m)* in the variables (y_1, y_2) are a priori assumed for the stress components. Since stresses are polynomial expressions, the generic ij^{th} component can be written as follows:

$$\sigma_{ij}^{(k,i_L)} = \mathbf{X}(\mathbf{y})\mathbf{S}_{ij}^{(k,i_L)T} \quad \mathbf{y} \in Y^{(k,i_L)} \tag{2}$$

where:

- $\mathbf{X}(\mathbf{y}) = \begin{bmatrix} 1 & y_1 & y_2 & y_1^2 & y_1 y_2 & y_2^2 & \dots \end{bmatrix}$;

- $\mathbf{S}_{ij}^{(k,i_L)} = \begin{bmatrix} S_{ij}^{(k,i_L)(1)} & S_{ij}^{(k,i_L)(2)} & S_{ij}^{(k,i_L)(3)} & S_{ij}^{(k,i_L)(4)} & S_{ij}^{(k,i_L)(5)} & S_{ij}^{(k,i_L)(6)} & \dots \end{bmatrix}$ is a vector representing the unknown stress parameters of sub-domain (k) of layer (i_L);

- $Y^{(k,i_L)}$ represents the kth sub-domain of layer (i_L).

The imposition of equilibrium (with zero body forces, as usually considered in homogenization procedures) inside each sub-domain, the continuity of the stress vector on interfaces and the anti-periodicity of $\boldsymbol{\sigma}\mathbf{n}$ permit directly a strong reduction of the total number of independent stress parameters.

Namely, the imposition of micro-stress equilibrium ($\sigma_{ij,j} = 0$ $i = 1,2$) in each sub-domain yields:

$$\sum_{j=1}^{2} \mathbf{X}(\mathbf{y})_{,j} \mathbf{S}_{ij}^{(k,i_L)T} = \mathbf{0} \tag{3}$$

If p is the degree of the polynomial expansion, $p(p+1)$ equations can be written.

A further reduction of total unknowns is obtained imposing a priori the continuity of the (micro)-stress vector on internal interfaces ($\sigma^{(k,i_L)}_{ij}n^{\text{int}}_j + \sigma^{(r,i_L)}_{ij}n^{\text{int}}_j = 0$ $i=1,2$) for every (k,i_L) and (r,i_L) contiguous sub-domains with a common interface of normal $\mathbf{n}^{\text{int}}$ (Figure 3-c). Therefore, additional $2(p+1)$ equations in the stress coefficients can be written for each interface as follows:

$$\left(\hat{\mathbf{X}}^{(k,i_L)}_{ij}(\mathbf{y})\hat{\mathbf{S}}^{(k,i_L)} + \hat{\mathbf{X}}^{(r,i_L)}_{ij}(\mathbf{y})\hat{\mathbf{S}}^{(r,i_L)T} \right) n^{\text{int}}_j = 0 \quad i=1,2 \tag{4}$$

Finally, anti-periodicity of $\boldsymbol{\sigma}\mathbf{n}$ on ∂V requires $2(p+1)$ additional equations per pair of external faces (m,i_L) and (n,i_L) (Figure 3-c), i.e. it should be imposed that stress vectors $\boldsymbol{\sigma}\mathbf{n}$ are opposite on opposite sides of ∂V:

$$\hat{\mathbf{X}}^{(m,i_L)}_{ij}(\mathbf{y})\hat{\mathbf{S}}^{(m,i_L)}\mathbf{n}_{1,j} = -\hat{\mathbf{X}}^{(n,i_L)}_{ij}(\mathbf{y})\hat{\mathbf{S}}^{(n,i_L)}\mathbf{n}_{2,j} \tag{5}$$

where $\mathbf{n}_1$ and $\mathbf{n}_2$ are oriented versors of the external faces of the paired sub-domains (m,i_L) and (n,i_L).

Some elementary assemblage operations on the local variables lead to the stress vector of layer i_L inside each sub-domain given by:

$$\tilde{\boldsymbol{\sigma}}^{(k,i_L)} = \tilde{\mathbf{X}}^{(k,i_L)}(\mathbf{y})\tilde{\mathbf{S}}^{(i_L)} \quad k=1,\dots,\text{ number of } sub-domains \, i_L=1,\dots,\text{number of } layers \tag{6}$$

where $\tilde{\mathbf{S}}^{(i_L)}$ is the vector of unknown stress parameters of layer i_L.

It is worth mentioning that equations (3), (4), (5) can be written in a compact form as $\mathbf{AS} = \mathbf{0}$, where $\mathbf{S}$ is the vector of total stress parameters and $\mathbf{A}$ is a matrix of geometrical coefficients with $\tilde{n}$ rows (expressing internal equilibrium in sub-domains, interface equilibrium between contiguous sub-domains and anti-periodicity) and $\tilde{m}$ columns (where $\tilde{m}$ is the total number of independent + dependent unknowns). Moreover, not all the rows of this system are linearly independent and the linear dependence of some equations with respect to others can be easily handled automatically (for instance by means of Symbolic Math Toolbox[TM]) checking the rank of matrix $\mathbf{A}$ and progressively eliminating linearly dependent rows.

Reliable results can be obtained if a third order polynomial expansion is chosen for the stress field. For this reason, in all the examples treated next, such approximation is adopted.

It is stressed that, once the polynomial degree is fixed, the out-of-plane model presented requires a subdivision (n_L) of the wall thickness into several layers (Figure 3-a), with an a priori fixed constant thickness $\Delta_{L_i} = h/n_L$ for each layer. In this way, the following simple (non) linear optimization problem is derived:

$$
\begin{cases}
& \max\{\lambda\} \\
& \text{such that}
\begin{cases}
\mathbf{N} = \int_{k,i_L} \widetilde{\boldsymbol{\sigma}}^{(k,i_L)} dV & (a) \\[2mm]
\mathbf{M} = \int_{k,i_L} y_3 \widetilde{\boldsymbol{\sigma}}^{(k,i_L)} dV & (b) \\[2mm]
\mathbf{M} = \begin{bmatrix} M_{xx} & M_{xy} \\ M_{xy} & M_{yy} \end{bmatrix} = \lambda \begin{bmatrix} \cos(\psi)\cos(\vartheta) & \sin(\vartheta) \\ \sin(\vartheta) & \sin(\psi)\cos(\vartheta) \end{bmatrix} & (c) \\[2mm]
\psi = [0; 2\pi] \quad \theta = [0; \pi/2] & (d) \\[2mm]
\widetilde{\boldsymbol{\sigma}}^{(k,i_L)} = \widetilde{\mathbf{X}}^{(k,i_L)}(\mathbf{y})\widetilde{\mathbf{S}} & (e) \\[2mm]
\widetilde{\boldsymbol{\sigma}}^{(k,i_L)} \in S^{(k,i_L)} \quad \boldsymbol{\sigma}^I \in S^I & (f) \\[2mm]
k = 1,\ldots, \text{number of } sub-domains;\ i_L = 1,\ldots, \text{number of } layers & (g)
\end{cases}
\end{cases}
\qquad (7)
$$

where:

- ψ and ϑ are spherical cooridinates in $M_{xx} - M_{yy} - M_{xy}$, given by $\tan(\vartheta) = \dfrac{M_{xy}}{\sqrt{\left(M_{xx}^2 + M_{yy}^2\right)}}$,

$\tan(\psi) = \dfrac{M_{yy}}{M_{xx}}$;

- $S^{(k,i_L)}$ denotes the (non-linear) strength domain of the constituent material (mortar or brick) corresponding to the kth sub-domain and i_L^{th} layer.

- S^I represents the bricks-mortar interfaces strength domain, see Figure 4 and Figure 3-c. As experimental evidences show, cracks usually occur at the joints, therefore it appears particularly suitable to assume a limited strength for brick-mortar interfaces. Basic failure modes for masonry with weak mortar are a mixing of sliding along the brick-mortar interface, direct tensile cracking of the interface and compressive crushing. Thus, a linearized Lourenço and Rots (1997) failure criterion seems particularly suited for the analysis near failure of bricks-mortar interfaces, merging in a unique criterion frictional failure (Mohr-Coulomb), a tension cut-off f_t and a compressive cap described by parameters f_c and Φ_2, see Figure 4.

- $\boldsymbol{\sigma}^I = \begin{bmatrix} \sigma^I & \tau^I \end{bmatrix}^T$ is the micro-stress vector acting on the interfaces, being σ^I the stress component acting perpendicularly to the interface and τ^I the tangential stress component.

- $\widetilde{\mathbf{S}}$ collects all the unknown polynomial coefficients (of each sub-domain, of each layer).

- λ is the direction of the ultimate bending moment in the $M_{xx} - M_{yy} - M_{xy}$ space (see Figure 5);

It is worth underlining here that:

- membrane actions are kept, for the sake of simplicity, constant and independent from load multiplier. Hence, for the analysis at collapse of panels reported next, in-plane actions affect

7

optimization only in the evaluation of M_{xx}, M_{yy}, M_{xy} strength domains. This assumption is usually acceptable since a fixed in-plane compressive load (regarded as permanent load) $N_{yy} = -N_0$ exists, the wall thickness is small and the collapse is obtained at relatively small out-of-plane displacements.

- Condition (f) of equation (7) is enforced, in each sub-domain, in correspondence of a rxq rectangular regular grid of "nodal points". The authors shown that reliable solutions can be obtained with a minimum of $3x3$ grids (see Milani et al. 2006c).

The non linearity of the terms $\tilde{\sigma}^{(k,i_L)} \in S^{(k,i_L)}$, due to the (possible) non-linearity of the strength functions of the components is easily avoided by means of a piecewise linear approximation of constituent materials strength domains (see e.g. Anderheggen and Knopfel 1972). On the other hand, it is worth noting that recent trends in limit analysis have demonstrated that the linearization of the strength domain can be circumvented using conic/semidefinite programming (e.g. Makrodimopoulos and Martin (2006), Krabbenhoft et al. 2007 and 2008). It has been demonstrated that, in terms of processing time, this tool is better than classic linear programming (LP). Both free (e.g. SeDuMi, http://sedumi.mcmaster.ca/) and commercial (e.g. www.mosek.com) standalone tools are nowadays available; nonetheless, since the aim of this paper is mainly concentrated on the structural aspects, the classic interior point LP routine available in MATLAB® is used for the sake of simplicity.

Finally, some limitations of the model are worth noting. The approach proposed is a multilayer procedure with no interaction between the layers. This is of course the simplest way to obtain a lower bound plate model, but raises questions on the fact that the solid medium behaves in the similar manner. Furthermore, it is suited only for running bond masonry, whereas there is no possibility to utilize the suggested approach for double wythes structures. A 3D equilibrated model (with the same subdivision into parallelepiped sub-domains) is under investigation by the authors, with the aim of applying it to multi-leaf structures subject to impacts.

3 The quadratic programming problem at a structural level

In the field of steel structures, basic theorems concerning rigid-plastic dynamics, as well as models devoted to the evaluation of the effect of impacts (including one degree of freedom so called "mode solutions") are well known, e.g. Martin (1964), Martin and Symonds (1965), Tamuzh (1962) and many others. The main hypotheses of such models are the following (see Capurso 1972a and 1972b, Cannarozzi and Laudiero 1976, and a more recent paper by Kim and Huh 2006):

1. rigid-perfectly plastic behavior of the material;
2. strain rate insensitivity of the yield stress;

8

3. negligible changes of the geometry during deformation.

These requirements are somewhat contradictory, since large energy inputs will tend to cause large displacements and high velocities sensibly affect the value of yield stress. In order to circumvent these limitations, extensions to rate dependent materials and large deformations problems were attempted in the first applications (Capurso 1972b and Martin 1972).

It has been shown in classic literature that rigid-plastic approaches perform well for ductile structural elements subjected to impact and that experimental data available can be fitted with sufficient accuracy (e.g. Bodner and Symonds 1962). As a consequence, rigid-perfect plasticity has been used by many authors in design practice to obtain a fast estimate (Martin and Symonds 1965, Komarov and Nemirovskii 1985) of deformations induced by dynamic loads.

For masonry structures subjected to static loads, following the pioneering work by Heyman (1969), limit analysis has been extensively utilized (e.g. Orduña and Lourenço 2005, Milani et al. 2006b), certainly representing the faster tool of analysis for complex structures (Milani et al. 2008).

In analogy to the static case, a rigid-plastic assumption for bricks and mortar joints is attempted here, with the aim of analyzing, with a simple and efficient tool, full walls subjected to impact.

When dealing with discretized structures by FEs, the analysis of rigid-plastic structures subjected to impulsive loading can be studied in the framework of a quadratic programming approach. In particular, within the class of all internal actions and accelerations that are dynamically and plastically admissible (i.e. obeying dynamic equilibrium and belonging to the class of internal actions connected with initial velocities, so representing a static formulation, see Martin 1964), the actual set minimizes, following the original definition given in Capurso (1972a), the second order kinetic energy of the structure, i.e.:

$$
\min\{\Omega(\ddot{\mathbf{u}})\} = \min\left\{\frac{1}{2}\ddot{\mathbf{u}}^T \mathbf{m} \ddot{\mathbf{u}}\right\}
$$

$$
\text{subject to} \begin{cases} \widetilde{\mathbf{B}}^T \widetilde{\boldsymbol{\Sigma}} = \mathbf{F}(t) - \mathbf{m}\ddot{\mathbf{u}} & (a) \\[2mm] \widetilde{\mathbf{A}}^{eq} \widetilde{\boldsymbol{\Sigma}} = \widetilde{\mathbf{b}}^{eq} & (b) \\[2mm] \widetilde{\mathbf{A}}^{in} \widetilde{\boldsymbol{\Sigma}} \leq \widetilde{\mathbf{b}}^{in} & (c) \end{cases} \qquad (8)
$$

where:

-   $\ddot{\mathbf{u}}$ is the vector of nodal accelerations. Following this notation, $\dot{\mathbf{u}}$ and $\mathbf{u}$ will indicate in the following respectively velocities and displacements nodal vectors.

-   $\widetilde{\boldsymbol{\Sigma}}$ is the assembled vector of elements internal actions;

-   $\mathbf{F}(t)$ is the external forces vector, generally dependent upon the time step under consideration;

-   $\mathbf{m}$ is the square matrix of masses, which typically are lumped at each nodal point;

-   $\widetilde{\mathbf{B}}$ is a matrix of coefficients that depends only on size and shape of finite elements utilized.

Considering a FE discretization of the body and assuming a piecewise linear yield surface for an element E, the set of admissible internal actions states can be expressed by the set of linear inequalities:

$$\left[-\mathbf{A}\boldsymbol{\Sigma}^E + \mathbf{b}\right]\begin{bmatrix}=\\\geq\end{bmatrix}[\mathbf{0}] \qquad (9)$$

where

- $\mathbf{A} = \left[\mathbf{A}^{eq};\ \mathbf{A}^{in}\right]$ is the matrix assembling the components of the outward unit normals to the linearized masonry failure surface hyperplanes.

- $\mathbf{b} = \left[\mathbf{b}^{eq};\ \mathbf{b}^{in}\right]^T$ represents the vector of the distance of each hyperplane from the origin.

- $\boldsymbol{\Sigma}^E$ is the vector of element E internal actions.

In equation (8), the superscript $\sim$ indicates assembled matrices and vectors corresponding respectively to local elements matrices and vectors. The set of equations (*a*) in the optimization problem (8) represents dynamic equilibrium condition. The principle of virtual work yields to the corresponding compatibility condition:

$$\tilde{\mathbf{B}}\dot{\mathbf{u}} - \tilde{\tilde{\boldsymbol{\varepsilon}}}_{pl} = \mathbf{0} \qquad (10)$$

where $\tilde{\tilde{\boldsymbol{\varepsilon}}}_{pl}$ is the assembled plastic strain rate vector.

It is interesting to notice that in equation (8), a partition of matrix $\mathbf{A}$ and vector $\mathbf{b}$ into equalities and inequality constraints is imposed. In particular, equality constraints represent points yielded in the previous time step, whereas inequalities stand for the points in which yielding can occur.

A so called "kinematic" formulation is also available Capurso (1972a). In particular, within the class of all accelerations and plastic multiplier rates that are kinematically admissible and obeying an associated flow rule (i.e. which comply with compatibility and with outward normal rule for the set of planes not activated by the initial velocities), the actual set minimizes the sum of the second order kinetic energy and the residual dissipation rate of the structure, i.e.:

$$\min\left\{\Xi\left(\ddot{\mathbf{u}},\ddot{\boldsymbol{\lambda}}\right)\right\} = \min\left\{\frac{1}{2}\ddot{\mathbf{u}}^T\mathbf{m}\ddot{\mathbf{u}} - \mathbf{F}(t)^T\ddot{\mathbf{u}} + \tilde{\mathbf{b}}^{IT}\ddot{\boldsymbol{\lambda}}\right\}$$

$$\text{subject to}\begin{cases}\tilde{\mathbf{B}}^I\ddot{\mathbf{u}} = \tilde{\mathbf{A}}^I\ddot{\boldsymbol{\lambda}} & (a)\\ \ddot{\boldsymbol{\lambda}} = \left[\ddot{\boldsymbol{\lambda}}_y^T\ \ \ddot{\boldsymbol{\lambda}}_r^T\right]^T & (b)\\ \ddot{\boldsymbol{\lambda}}_r \geq \mathbf{0} & (c)\end{cases} \qquad (11)$$

where:

- $\ddot{\boldsymbol{\lambda}}$ is the vector of second derivatives of plastic multipliers (in the present case plastic multipliers are referred to each interface). $\ddot{\boldsymbol{\lambda}} = \left[\ddot{\boldsymbol{\lambda}}_y^T\ \ \ddot{\boldsymbol{\lambda}}_r^T\right]^T$ is the partitioned $\ddot{\boldsymbol{\lambda}}$ vector, where index y

indicates that the corresponding $\dot{\lambda}_y \neq 0$, whereas index r indicates that at the previous iteration $\dot{\lambda}_r = 0$;

- The superscript I indicates quantities (i.e. vectors and matrices) referred to interfaces. It is worth noting that the procedure outlined by Krabbenhoft et al. (2005), was adopted to obtain homogenized masonry strength domains (and hence vectors and matrices in the rotated frame of reference) for an interface with generic orientation ϑ^I with respect to horizontal axis.

More in detail, if the vector $\boldsymbol{\lambda}^E = \begin{bmatrix} \lambda_1^E & \lambda_2^E & \dots & \lambda_n^E \end{bmatrix}^T$ represents plastic multipliers of an element E (or an interface I), the associated flow rule is expressed for each element as:

$$\dot{\boldsymbol{\varepsilon}}_{pl}^E = \mathbf{A}^T \dot{\boldsymbol{\lambda}}^E \tag{12}$$

where $\dot{\boldsymbol{\varepsilon}}_{pl}^E$ is the plastic strain rate vector of element E. In the framework of rigid-perfect plasticity, equation (12) is subjected to the following equality and inequality constraints:

$$\begin{cases} \dot{\boldsymbol{\lambda}}^E \geq \mathbf{0} \\ \left(\dot{\boldsymbol{\lambda}}^E\right)^T \left(-\mathbf{A}\boldsymbol{\Sigma} + \mathbf{b}\right) = 0 \end{cases} \tag{13}$$

u with its derivatives with respect to time is a function of time, $\dot{\boldsymbol{\varepsilon}}_{pl}^E$ and $\dot{\boldsymbol{\lambda}}^E$ are also time dependent functions. Thus, differentiation of equation (12) with respect to time yields:

$$\ddot{\boldsymbol{\varepsilon}}_{pl}^E = \mathbf{A}^T \ddot{\boldsymbol{\lambda}}^E \tag{14}$$

Element E (or an interface I), which is governed by plastic flow law (12), (13) and (14), at a given instant t_0 is in one of the following four cases:

1. if the internal actions vector $\boldsymbol{\Sigma}^E$ is inside the failure surface, then $\dot{\boldsymbol{\varepsilon}}_{pl}^E = \mathbf{0}$, implying that:

    $$\dot{\boldsymbol{\lambda}}^E = \ddot{\boldsymbol{\lambda}}^E = \mathbf{0} \tag{15}$$

    with an undetermined state for the internal actions state.

2. if the internal actions vector is a regular point of the linearized failure surface (say belonging to the j th hyperplane), but $\dot{\boldsymbol{\lambda}}^E(t_0) = \mathbf{0}$, one has:

    $$\begin{cases} \dot{\boldsymbol{\lambda}}^E = \mathbf{0} \\ \ddot{\lambda}_j^E \geq 0 \\ \ddot{\lambda}_{i \neq j}^E = 0 \end{cases} \tag{16}$$

3. if the internal actions vector is a regular point of the linearized failure surface belonging to the j th hyperplane) and $\dot{\boldsymbol{\lambda}}^E(t_0) \neq \mathbf{0}$, one has:

$$\begin{cases} \dot{\lambda}_j^E > 0 \\ \dot{\lambda}_{i \neq j}^E = 0 \\ \ddot{\lambda}_j^E \quad \text{free} \\ \ddot{\lambda}_{i \neq j}^E = 0 \end{cases}$$

(17)

4. if the internal actions vector is a singular point of the linearized failure surface common to m hyperplanes, one has:

$$\forall \alpha \in [1 \ \dots \ m] \begin{cases} \ddot{\lambda}_\alpha^E \geq 0 & if \ \dot{\lambda}_\alpha^E = 0 \\ \ddot{\lambda}_\alpha^E & free \ if \ \dot{\lambda}_\alpha^E > 0 \end{cases}$$

(18)

In cases 2 and 3 the internal action vector is represented by any point of the jth hyperplane, whereas for case 4 the internal action state is uniquely determined.

The assembly of all elements transfers the qualitative behavior of a single element (or an interface) to the overall discretized structure. Hence, the assembled stress state $\tilde{\Sigma}$ is constant during finite time intervals. If the vector of external loads is assumed constant during finite time intervals, it can be shown (Cannarozzi and Laudiero 1976) that the most general motion of a rigid plastic structure is a sequence of uniformly accelerated motions of finite time interval. The interchange of two consecutive mechanisms is characterized by a discontinuity of the acceleration fields.

Therefore, the set of active yield planes of each element at a given time t_0 is known. For a time step of duration Δt we have:

$$\begin{aligned} \dot{\lambda}_y > \mathbf{0} \\ \dot{\lambda}_r = \mathbf{0} \end{aligned}$$

(19)

where the subscript y (r) denotes the vector collecting all the non-zero (zero) plastic multiplier rates in the structure, indicating if a yielding condition for a certain element has (has not) been reached. From the previous considerations, differentiation of equation (19) yields:

$$\begin{aligned} \ddot{\lambda}_y \text{free} \\ \ddot{\lambda}_r \geq \mathbf{0} \end{aligned}$$

(20)

Finally, the following assembled equation representing the first derivative associated flow rule condition is obtained:

$$\tilde{\ddot{\varepsilon}}_{pl} - \begin{bmatrix} \tilde{\mathbf{A}}^{eqT} & \tilde{\mathbf{A}}^{inT} \end{bmatrix} \begin{bmatrix} \ddot{\lambda}_y \\ \ddot{\lambda}_r \end{bmatrix} = 0$$

(21)

where the aforementioned partition of matrix $\tilde{\mathbf{A}}$ is introduced. Exploiting equation (10), a relation between accelerations and second derivatives of plastic multipliers is obtained in the form:

$$\mathbf{B}\widetilde{\mathbf{u}} - \begin{bmatrix} \widetilde{\mathbf{A}}^{eqT} & \widetilde{\mathbf{A}}^{inT} \end{bmatrix} \begin{bmatrix} \ddot{\boldsymbol{\lambda}}_y \\ \ddot{\boldsymbol{\lambda}}_r \end{bmatrix} = 0 \tag{22}$$

with corresponding static conditions:

$$\begin{cases} \widetilde{\mathbf{A}}^{eq}\widetilde{\boldsymbol{\Sigma}} = \widetilde{\mathbf{b}}^{eq} \\ \widetilde{\mathbf{A}}^{in}\widetilde{\boldsymbol{\Sigma}} \le \widetilde{\mathbf{b}}^{in} \\ \widetilde{\boldsymbol{\lambda}}_r \left(\widetilde{\mathbf{A}}^{in}\widetilde{\boldsymbol{\Sigma}} - \widetilde{\mathbf{b}}^{in} \right) = 0 \end{cases} \tag{23}$$

Previous conditions (12)-(21), from well known connections between linear complementarity problems and quadratic programming lead to the formulation reported in (8).

4 The FE thin plate triangular formulation

In order to solve low velocity impact problems for out-of-plane loaded masonry structures, a FE thin plate triangular formulation based on the plate bending element proposed independently by Hellan (1967) and Herrmann (1967) is used. This triangular element has been preferred to more accurate elements present in the literature (Krabbenhoft and Damkilde 2002, Krenk et al. 1994), due to its simplicity and the low number of unknowns involved in the optimization.

A constant moment field is assumed inside each element E, so that three moment unknowns per element are introduced. The unknowns are the horizontal, vertical and torsion moments ($M_{xx}^E, M_{yy}^E, M_{xy}^E$) or alternatively three bending moments M_{nn}^{Ei}, M_{nn}^{Ej}, M_{nn}^{Ek} along the edges of the triangle (Figure 6-a).

For what concerns the displacement field, the element turns out to be analogous to the Munro and Da Fonseca (1978) triangle. In particular, the displacement field is assumed linear inside each element and nodal displacements are taken as optimization variables. Denoting by $\mathbf{w}_E = \begin{bmatrix} w_i^E & w_j^E & w_k^E \end{bmatrix}^T$ the element E nodal displacements and by $\boldsymbol{\theta}_E = \begin{bmatrix} \vartheta_i^E & \vartheta_j^E & \vartheta_k^E \end{bmatrix}^T$ the side normal rotations, $\boldsymbol{\theta}_E$ and $\mathbf{w}_E$ are linked by the compatibility equation (Figure 7-a and –b):

$$\boldsymbol{\theta}_E = \mathbf{B}_E \mathbf{w}_E \tag{24}$$

where:

- $\mathbf{B}_E = \dfrac{1}{2A_E} \begin{bmatrix} \dfrac{b_i b_i + c_i c_i}{l_i} & \dfrac{b_i b_j + c_i c_j}{l_i} & \dfrac{b_i b_k + c_i c_k}{l_i} \\ \dfrac{b_j b_i + c_j c_i}{l_j} & \dfrac{b_j b_j + c_j c_j}{l_j} & \dfrac{b_j b_k + c_j c_k}{l_j} \\ \dfrac{b_k b_i + c_k c_i}{l_k} & \dfrac{b_k b_j + c_k c_j}{l_k} & \dfrac{b_k b_k + c_k c_k}{l_k} \end{bmatrix}$, with $b_i = y_j - y_k$, $c_i = x_k - x_j$ and A_E is

the element area.

Therefore, plastic dissipation occurs only at the interface I between two adjacent triangles R and K or on a boundary side B of an element Q (see Figure 7-c). Continuity of M_{nn}^{E} bending moments is imposed for each internal interface between two adjacent elements R and K (i.e. $M_{nn}^{Ri} = M_{nn}^{Kj}$, see Figure 6-b), whereas no constraints are imposed for the torsion moment and the shear force.

Due to the constant assumption for the moment fields, internal equilibrium for each element is ensured in integral form. By means of the application element by element of the principle of virtual work, three equilibrium equations for each triangle are obtained:

$$\mathbf{R}_E + \mathbf{B}_E^T \mathbf{M}_E = \mathbf{P}_E + \mathbf{M}\ddot{\mathbf{w}}_E \qquad (25)$$

where

- $\mathbf{R}_E = \begin{bmatrix} R_i & R_j & R_k \end{bmatrix}^T$ are nodal (unknown) reactions, see Figure 6-c;

- $\mathbf{P}_E = \dfrac{1}{2A_E}\mathbf{T}_E^T \int_E \begin{bmatrix} 1 & x & y \end{bmatrix}^T p(x,y)dA$ ($\mathbf{T}_E^T = \begin{bmatrix} a_i & a_j & a_k \\ b_i & b_j & b_k \\ c_i & c_j & c_k \end{bmatrix}, a_i = x_j y_k - x_k y_j$). It is interesting to notice that vector $\mathbf{P}_E$ can be regarded as a lumped load equivalent to the resultant action associated to $p(x,y)$.

- the term $\mathbf{M}\ddot{\mathbf{w}}_E$ includes the contribution of inertia forces to the overall equilibrium. Matrix $\mathbf{M}$ is the matrix of equivalent lumped masses and is obtained analogously to vector $\mathbf{P}_E$ assuming a constant density ρ inside each triangular element.

In order to find the duration Δt of the time interval to discretize equation (25), it is worth noting that:

$$\dot{\boldsymbol{\lambda}}_y(t) = \dot{\boldsymbol{\lambda}}_y^0(t_0) + \ddot{\boldsymbol{\lambda}}_y^0(t - t_0)$$
$$\dot{\boldsymbol{\lambda}}_r = \ddot{\boldsymbol{\lambda}}_r^0(t - t_0) \qquad (26)$$

where subscript 0 refers to quantities calculated in the previous iteration. Since each component of vector $\dot{\boldsymbol{\lambda}}_{y,r}$ has to be non-negative, the duration Δt of the interval chosen is therefore:

$$\Delta t = \min\left\{(t - t_0) \text{ such that } \dot{\boldsymbol{\lambda}}_y^0\big|_{\bar{i}}(t_0) + \ddot{\boldsymbol{\lambda}}_y^0\big|_{\bar{i}}(t - t_0) = 0\right\} \qquad (27)$$

where the subscript $\bar{i}$ indicates a generic element of the vectors $\dot{\boldsymbol{\lambda}}_y^0$ and $\ddot{\boldsymbol{\lambda}}_y^0$.

Further equality constraints have to be imposed in order to ensure nodal equilibrium, i.e. for each (not-constrained) node i the following equation has to be satisfied:

$$\sum_{r=1}^{p} R_i^E = 0 \qquad (28)$$

where R_i^E is referred to element E and p is the number of elements with one vertex in i.

Since moment fields are kept constant for each element E, only one set of admissibility conditions in the linearized form $\mathbf{A}_E^{in}\mathbf{M}_E \leq \mathbf{b}_{in}^E$ is required, where $\mathbf{A}_E^{in}$ is a $mx3$ coefficients matrix of the linearization planes of the strength domain, m is the number of the planes in the linearization, $\mathbf{b}_{in}^E$ collects the right hand sides of these planes and $\mathbf{M}_E = \begin{bmatrix} M_{xx}^E & M_{yy}^E & M_{xy}^E \end{bmatrix}^T$ is the vector of element moment unknowns.

It is interesting to notice that assembled equations (25) and (28) correspond to equilibrium equation (8)-(a), whereas moments admissibility at each time step corresponds to constraints (8)-(b) and (c).

The algorithm used to numerically solve the quadratic programming problem (8)-(11) is a modification of the revised simplex method, applied to the LCP problem obtained from (8), by means of the application of Kuhn-Tucker conditions. Details of the algorithm can be found in Jensen and Bard (2003).

5 Numerical simulations

Two examples are presented, in order to assess the capabilities of the model proposed when compared to alternative numerical results obtained by means of standard commercial non-linear FE codes and, where available, to experimental results from the literature.

It is noted that the topic has been under-investigated, both from an experimental and numerical point of view. Therefore, the main goal of the present paper is to provide structural comparisons with approaches that may be utilized by practitioners in design.

As a secondary result, comparisons with experiments, when available, have been attempted, obviously considering that a rigid-plastic model is able to perform well in presence of low mechanical properties for the constituent materials or by assuming an "equivalent" reduced tensile strength.

The first example is a masonry parapet arranged in running bond texture experimentally and numerically tested by Gilbert et al. (1998, 2002a and 2002b) and Burnett et al. (2007). The wall is subjected to a low velocity impact simulating the crush of a car on a masonry parapet. Comparisons with experimental data available (Gilbert et al. 1998), numerical simulations by Burnett et al. (2007) and 2D/3D elastic-plastic heterogeneous FE analyses conducted by means of the commercial software Strand 7.2 (2004) are reported, in order to show that reliable results can be obtained with the model proposed.

Since experimentally determined mortar tensile strength is, in this case, relatively high, numerical rigid-plastic time-displacement response may be compared with experimental data only assuming

an ad-hoc reduced value for f_t . With this aim, a sensitivity analysis is conducted by varying f_t in a wide range. Thanks to the very small CPU time required for the rigid-plastic simulations, multi-parameters sensitivity analyses are possible.

The second example is a square plate constrained at four edges, subject to a dynamic load simulating an air-blast (Wu and Hao 2006 and 2008). Experimental data are missing in this case, as well as precise time-displacement curves from numerical simulations. A similar simulation with time-displacement curves available (at least for a rough estimation of the performance of the present simple model with respect to complex non linear analyses) may be found in Wang et al. (2009). For this reason, similarly to the previous case, the rigid-plastic model is compared with heterogeneous 2D and 3D elastic-plastic Strand 7.2 models.

For both examples, maximum displacement-time diagrams show that reliable results (in comparison with standard 2D/3D FE approaches) can be obtained with the homogenized model proposed. On the other hand, a proper experimental validation of the approach presented is not possible, due to the lack of experimentation in this field, especially in presence of mortar with low mechanical properties.

5.1 Masonry parapet subjected to point low velocity impact

The performance of brickwork parapets subjected to a low velocity impact simulating a car crash was numerically and experimentally evaluated respectively by Burnett et al. (2007) and Gilbert et al. (2002a). Analytical simplified approaches are also available from Gilbert et al. (2002b). Several parapets differing in length and bricks disposition (stretcher, English and English Garden bond) were tested (see Burnett et al. 2007, Gilbert et al. 1998, 2002a and 2002b for details). Here, for the sake of conciseness, only the running bond configuration (two replicates labeled as C6 and C7 by Gilbert et al. 2002a) is considered. In particular, walls C6 and C7 are identical stretcher bond parapets with dimensions 9150×1130×215 mm (length × height × thickness) built with highly resistant concrete blocks of dimensions 440×215×215 mm (length × height × thickness) and approximately 10 mm thick joints, see Figure 8. The parapet was subjected to an out-of-plane car like impact, applied by means of a square steel plate positioned in correspondence of the mid-length. Two stiff concrete abutments were positioned at the extremes of the wall, thus precluding the rotation of the vertical edges. The first row of blocks was directly positioned in correspondence of a stiff steel floor, thus allowing (at least in principle) a free rotation of the horizontal edge.

For the numerical simulations, a triangular time-load distribution was assumed, with a peak value equal to 110 kN reached at 25msec, see Figure 8, approximating the experimentally registered load applied.

In the numerical simulations conducted by Burnett et al. (2007), a heterogeneous approach with joints reduced to interfaces with frictional behavior and elliptic tensile cap failure criterion, with bricks assumed as linear elastic, was adopted. Post peak joints behavior was found with a marked softening branch, whereas for the initial tensile and shear strength, relatively high values (0.45 MPa and 0.63 MPa respectively) were used. If such a high value of tensile strength is adopted in the rigid-plastic approach here proposed, dissipation occurring in joints is obviously overestimated, with a consequent underestimation of displacements at increasing time steps. This behavior is typical for a rigid-perfectly plastic approach, where it is not possible to model the well known softening behavior in tension of the mortar joints.

As discussed above, the model proposed may approximate well experimental data in presence of joints with poor mechanical properties or assuming a reduced tensile strength for mortar, thus simulating masonry behavior after initial cracking of joints (see the numerical simulations reported in Hamad and Rabinovitch 2008).

In order to have a better insight into the global behavior of the parapet using the model proposed, two different sets of mechanical properties for bricks-mortar interface tensile and shear strength are assumed, as summarized in Table I. As it is possible to notice from the table, tensile strength values adopted are lower with respect to Gilbert et al. (2002a). The goal of the simulations is, indeed, to show that, when cracking of joints has occurred, the behavior of the walls can be satisfactorily reproduced with the model proposed, provided that particular care is utilized in the evaluation of input mechanical properties. In order to cover a sufficiently large range of cases, a relatively low tensile strength is assumed for CASE A (approximating a scarcely tensile resistant material), whereas for CASE B the simulations are repeated supposing a higher strength for brick-mortar interfaces (typically ranging between 1/2 and 1/5 of the initial strength). For bricks and joints sub-domains, a classic Mohr-Coulomb failure criterion in plane stress is adopted (bricks cohesion is 2 MPa, bricks friction angle is $\Phi = 45°$, mortar cohesion is $c = 0.63$ MPa, and mortar friction angle is $\Phi = 38°$ [data collected from Burnett et al. 2007]).

At structural level, both a shell (hereafter named as 2.5D) and a 3D FE heterogeneous elastic-plastic dynamic analysis have been conducted, in order to have adequate insight into the problem and to collect results to compare with those provided by the present rigid-plastic approach.

The two different heterogeneous meshes utilized in the 2.5 and 3D case are depicted in Figure 9-b and -c respectively, together with the homogenized mesh adopted, shown in Figure 9-a. Models will be denoted hereafter respectively with labels WI2.5D and WI3D for the sake of simplicity.

For both WI2.5D and WI3D models, the commercial software Strand 7.2 (2004) was utilized to perform the dynamic non-linear analyses. As shown in Figure 9, a relatively refined discretization

was adopted for WI2.5D and WI3D, in order to avoid possible inaccuracies due to mesh dependence. A Mohr-Coulomb failure criterion was used for bricks (with the same properties of the rigid plastic model proposed), whereas for joints a Mohr-Coulomb failure criterion with the tensile strength and friction angle of bricks-mortar interfaces used in the homogenized approach was adopted. It is worth noting that, for model WI2.5D, elastic-plastic eight-noded quadrilateral elements were used in order to prevent possible numerical inaccuracies due to locking phenomenon in bending. For WI3D model, eight-noded brick elements were utilized both for joints and bricks, with a double row of elements along wall thickness.

A comparison among the deformed shapes at t=100 msec obtained with the present model, WI2.5D and WI3D is schematically depicted in Figure 10 (CASE A results are shown). As it is possible to notice, all models give almost the same response in terms of deformed shape for the particular instant time inspected (100 msec), except for the presence of a slight out-of-plane sliding at the base of the wall (particularly evident in the model WI3D), which obviously cannot be reproduced with simple Kirchhoff-Love approaches as the one presented in this paper.

It is worth noting that the homogenized rigid plastic model required only 252 seconds to be performed on a standard PC Intel Celeron 1.40 GHz equipped with 1Gb RAM, a processing time around 100 and 200 faster than WI2.5D and WI3D respectively. Due to the very limited computational effort required, full sensitivity analyses are possible even for complex structures.

In Figure 11 and Figure 12, the response of the homogenized rigid-plastic model when subjected to the aforementioned impact load is reported for CASE A and CASE B respectively. In particular, maximum out-of-plane displacements at increasing time steps as well as the evolution of the deformation at successive instants are represented graphically.

A full comparison among maximum out-of-plane displacement at the mid-length top point of the wall at increasing time obtained with the different models previously described is reported in Figure 13. Results obtained adopting a simplified model based on the a-priori assumption of rigid body motion with dissipation on interfaces between contiguous bodies (Gilbert et al. 2002b) are also represented. It is interesting to notice that wall deformation depends significantly on cohesion and tensile strength of bricks-mortar interfaces, confirming that the selection of mechanical properties is a key issue. In any case, if compared with standard elastic-plastic procedures, the model adopted seems to provide quite accurate results, at a fraction of the time of non-linear dynamic FE simulations.

Finally, in Figure 14, sensitivity analysis results are reported ranging tensile strength from 0.1 to 0.3 MPa. In particular, the maximum out-of-plane displacement (at the end of the simulations, i.e. 200 msec) obtained with the model proposed at increasing f_t is depicted. As expected, maximum

displacement decreases significantly when high strength mortar is adopted. Furthermore, from the sensitivity analysis shown, a value of f_t around 0.2 MPa provides optimal experimental data fitting. From the results reported in Figure 14 and remembering previous considerations and limitations, it can be stated that a rigid plastic model can be adopted to analyze masonry structures subjected to low velocity impacts, giving interesting information on displacement-time curves, provided that a careful analysis of input mechanical properties is done (i.e. in the range of the low values suggested by codes of practice).

5.2 Square masonry plate subjected to air-blast load

A simply supported masonry plate of dimensions 200 × 180 cm (length × height), built with hollow concrete units of dimensions 390×190×190 mm (length × height × thickness) and subjected to an air-blast load is here considered as a second example. A similar example has been numerically analyzed by Wu and Hao in (2008), where a deep discussion on aspects related to masonry cracking during air-blast was reported. No information on the maximum displacement at successive time steps to compare to present FE results is at disposal from Wu and Hao (2008), therefore the example here treated is aimed at testing the capabilities of the model proposed when compared with FE standard codes only (i.e. without specific reference to Wu and Hao 2006 and 2008). Furthermore, no experimental data are available in the technical literature for this example. A similar example with time-maximum displacement numerical diagrams on a square masonry plate subjected to blast is discussed in Wang et al. (2009). Magnitude of maximum displacement at the end of the simulations as well as displacements at increasing time steps result in very good agreement with simulations presented in this section (even if only a qualitative comparison is possible in this case), confirming the capabilities of the model proposed (for further details the reader is referred to Wang et al. 2009).

In order to collect numerical results and with the aim of assessing the data provided by the homogenization model proposed, analogously to the previous example, two different heterogeneous FE dynamic elastic-plastic analyses have been performed by means of the commercial code Strand 7.2. As in the previous case, a 2D and a 3D approach, hereafter labeled as WII2.5D and WII3D, have been adopted. Mesh WII2.5D is constituted by quadrilateral plates, whereas WII3D by solid brick elements. Figure 16 shows the discretization adopted for the simulations.

Again, for model WII2.5D, elastic-plastic eight-noded elements were used, whereas for WII3D a double row of eight-noded brick elements was disposed along wall thickness in order to reproduce out-of-plane bending. WII3D constraints have been applied at the boundary nodes belonging to the

intrados, in order to avoid a fictitious extra-resistance of mortar joints caused by the possible presence of membrane compressive stresses at the middle surface.

Wu and Hao (2008) assumed for mortar joints and bricks a tensile strength equal to 1 MPa and 2.6 MPa respectively. As in the previous example, joints initial tensile strength is rather high. Furthermore, in Wu and Hao (2008), a marked softening branch in tension is assumed, with the consequent reduction of f_t almost to zero immediately after first cracking of the joint. Obviously, such behavior cannot be reproduced with the model here proposed.

In order to circumvent this drawback, a sensitivity analysis is performed next, assuming for bricks-joints interfaces two different tensile strength values, hereafter denoted as CASE A and B, respectively equal to 0.2 and 0.5 MPa (typically 1/5 and ½ of initial strength).

For all the cases analyzed and for all the simulations conducted, a Rankine failure criterion is adopted for bricks with tensile and compressive strength equal to 2.6 MPa and 52 MPa, whereas for mortar sub-domains a Mohr-Coulomb failure criterion is assumed with f_t =1 MPa and Φ =30° (data collected from Wu and Hao 2008). When dealing with the rigid-plastic homogenization model, a linearization of the failure criterion originally proposed in Lourenço and Rots (1997), see Figure 3, is assumed for brick-joint interfaces, see Table II for a synopsis of all the mechanical properties adopted. On the other hand, two different analyses on WII2.5D and WIII3D models have been conducted, assuming a Mohr-Coulomb failure criterion with decreasing cohesion $c = f_f \tan(\Phi)$ for mortar, f_t values as in Table II and $\Phi = 30°$.

In Figure 17, a comparison among deformed shapes at t=10msec provided by the present model, WII2D and WII3D in Case A is reported. As it is possible to notice, all models give almost the same response in terms of deformed shape for the particular instant time inspected. No sensible differences among all models were found varying both time and mortar mechanical properties.

Analogously to the previous example, processing time required for the present rigid-plastic simulations was at least 180 times faster when compared with standard commercial code, confirming that reliable results can be obtained with a fraction of the computational effort.

In Figure 18 and Figure 19, the deformation evolution at different time steps and the maximum-displacement-time diagram up to 0.06 sec from the rigid-plastic analysis are represented respectively for CASE A and CASE B.

A final synopsis of all time-central point displacement diagrams obtained by means of the different FE approaches presented previously and assuming different mechanical properties for the constituent materials is reported in Figure 20, carrying out the simulations to 100 msec. Furthermore, in Figure 20, results obtained adopting a simplified model based on a yield line solution and originally proposed by Komarov and Nemirovskii (1985) are also represented. Such

approach is based essentially on rigid-plastic assumptions for the material, thus it is expected that it provides results in relative agreement with the homogenized model proposed. As already pointed out, no information is at disposal from the literature with respect to numerical displacements at the centre of the plate at successive time steps, and experimental data are missing. In any case, comparisons with standard FE elastic-plastic approaches conducted via a commercial software and hand calculations clearly show that very reasonable results may be obtained by means of the homogenization rigid plastic model proposed.

6 Conclusions

A homogenized rigid-plastic plate model for the analysis of masonry plates subjected to impacts and air-blasting has been presented. Bricks and mortar joints have been assumed obeying an associated flow rule with rigid perfectly plastic behavior. Out-of-plane anisotropic masonry failure surfaces have been obtained by means of a static limit analysis approach recently presented in Milani et al. (2006c), in which the unit cell is subdivided into a fixed number of sub-domains and layers along the thickness. A limited strength (frictional failure with compressive cap and tension cutoff) of brick-mortar interfaces has been also taken into account, thus making the reproduction of elementary cell failures due to the insufficient resistance of the bond between units and joints possible.

Triangular Kirchhoff-Love elements with linear interpolation of the displacements field and constant moment within each element have been used at a structural level, leading to a discretized quadratic programming formulation at each time step for the analysis of entire walls subjected to impacts.

Two examples have been treated, namely a running bond masonry wall constrained at three edges and subjected to a point impact load and a masonry square plate constrained at four edges and subjected to a distributed dynamic pressure.

While for the first example some experimental data are available, the second analysis may be compared only with alternative numerical procedures conducted with commercial software available in the market stock.

Comparisons with experiments (where available) may be attempted only taking into account that rigid-plastic models perform well if softening is not crucial, i.e. in presence of low mechanical properties for the constituent materials, or alternatively after joints first cracking, i.e. assuming an "equivalent" reduced tensile strength for mortar.

For these reasons, the primary aim of the approach proposed is to provide structural comparisons with alternative commercial FE non linear software, usually available in common design.

For all the simulations performed, the model proposed required a negligible processing time if compared with standard FE incremental procedures, as represented in Table III, where a synopsis of CPU times required and maximum displacements at the end of the simulations for both examples is reported. As one can note from maximum displacements reported in Table III, good agreement has been found, for all the cases analyzed, both with standard elastic-plastic FE procedures and at hand calculations. Finally, Table III results indicate that the proposed simple tool can be used by practitioners (parallely to alternative sophisticated approaches) for the safety assessment of out-of-plane loaded masonry panels subjected to impacts, at a very small fraction of the time used for conventional finite element analysis.

7 References

[1]   Anderheggen E, Knopfel H (1972). Finite element limit analysis using linear programming. International Journal of Solids and Structures; 8: 1413-1431.

[2]   Astbury NF, West HWH, Hodgkinson HR, Cubbage PA, Clare R (1970). Gas explosions in load bearing brickwork structures. BCRA special publication 68, Stoke on Trent.

[3]   Bodner RS, Symonds PS (1962). Experimental and theoretical investigation of the plastic deformation of cantilever beams subjected to impulsive loading. Journal of Applied Mechanics; 719.

[4]   British Standard Institution (1985). BS 5628: Use of Masonry.

[5]   Burnett S, Gilbert M, Molyneaux T, Beattie G, Hobbs B (2007). The performance of unreinforced masonry walls subjected to low-velocity impacts: Finite element analysis. International Journal of Impact Engineering; 34: 1433-1450.

[6]   Cannarozzi AA, Laudiero F (1976). On plastic dynamic flexure of plates. Meccanica; December: 208-218.

[7]   Capurso M (1972a). A quadratic programming approach to the impulsive loading analysis of rigid plastic structures. Meccanica; March: 45-57.

[8]   Capurso M (1972b). Minimum principles in the dynamics of isotropic rigid-plastic and rigid-viscoplastic continuous media. Meccanica; 7(2): 92-97.

[9]   Cecchi A, Milani G (2008). A kinematic FE limit analysis model for thick English bond masonry walls. International Journal of Solids and Structures; 45: 1302-1331.

[10]   EN 1991-1-7:2006 (2006). Eurocode 1 - Actions on structures - Part 1-7: General actions - Accidental actions.

[11]   EN 1996-1-1:2005 (2005). Eurocode 6 - Design of masonry structures - Part 1-1: General rules for reinforced and unreinforced masonry structures

[12] Gilbert M, Hobbs B, Molyneaux TCK, Melbourne C, Watson AJ (1998). Laboratory impact testing of free standing masonry walls. Masonry International; 11(3): 71-79.

[13] Gilbert M, Hobbs B, Molyneaux TCK (2002a). The performance of unreinforced masonry walls subjected to low-velocity impacts: experiments. International Journal of Impact Engineering; 27: 231-251.

[14] Gilbert M, Molyneaux TCK, Hobbs B (2002b). The performance of unreinforced masonry walls subjected to low-velocity impacts: mechanisms analysis. International Journal of Impact engineering; 27: 253-275.

[15] Hamed E, Rabinovitch O (2008). Masonry walls strengthened with composite materials - dynamic out-of-plane behaviour. European Journal of Mechanics/A Solids; 27: 1037–1059.

[16] Hellan K (1967). Analysis of elastic plates in flexure by a simplified finite element method. Acta Polytech. Scand., Trondheim; Ci 46: 1-28.

[17] Herrmann LR (1967). Finite element bending analysis for plates. J. Eng. Mech. Div. ASCE; 93: 13-26.

[18] Heyman J (1969). The safety of masonry arches. International Journal of Mechanical Sciences; 43: 209-224.

[19] Jensen PA, Bard JF (2003). Operations Research Models and Methods. John Wiley and Sons.

[20] Kim KP, Huh H (2006). Dynamic limit analysis formulation for impact simulation of structural members. International Journal of Solids and Structures; 43(21): 6488-6501.

[21] Komarov KL, Nemirovskii YV (1985). Dynamic behavior of rigid-plastic rectangular plates. International Applied Mechanics; 21(7): 69-76.

[22] Krabbenhoft K, Damkilde L (2002). Lower Bound limit analysis of slabs with nonlinear yield criteria. Computers and Structures; 80: 2043-2057.

[23] Krabbenhoft K, Lyamin AV, Hjiaj M, Sloan SW (2005). A new discontinuous upper bound limit analysis formulation. International Journal for Numerical Methods in Engineering; 63: 1069-1088.

[24] Krabbenhoft K, Lyamin AV, Sloan SW (2007). Formulation and solution of some plasticity problems as conic programs, International Journal of Solids and Structures; 44: 1533-1549.

[25] Krabbenhoft K, Lyamin AV, Sloan SW (2008). Three-dimensional Mohr-Coulomb plasticity using semidefinite programming, Communications in Numerical Methods in Engineering; 24(11): 1107-1119.

[26] Krenk S, Damkilde L, Hoyer O (1994). Limit analysis and optimal design of plates with equilibrium elements. J. Eng. Mech. ASCE; 120(6): 1237-1254.

[27] Lourenço PB, Rots J (1997). A multi-surface interface model for the analysis of masonry structures. Journal of Engineering Mechanics ASCE; 123(7): 660-668.

[28] Lourenço PB, de Borst R., Rots JG (1997). A plane stress softening plasticity model for orthotropic materials. International Journal for Numerical Methods in Engineering; 40: 4033-4057.

[29] Makrodimopoulos A, Martin CM (2006). Lower bound limit analysis of cohesive-frictional materials using second-order cone programming. International Journal for Numerical Methods in Engineering; 66 (4): 604-634.

[30] Martin JB (1964). Impulsive loading theorems for rigid-plastic continua. Proc. Eng. Mech. Div. ASCE; E.M. 5 90: 27.

[31] Martin JB, Symonds PS (1965). Mode approximations for impulsively loaded rigid-plastic structures. Brown University Report, Division on Engineering, Providence; 1-61.

[32] Martin JB, Ponter AS (1972). Bounds on large deformations of impulsively loaded elastic-plastic structures. Proc. ASCE; EM1: 107.

[33] Mayrhofer C (2002). Reinforced masonry walls under blast loading. International Journal of Mechanical Sciences; 44: 1067-1080.

[34] Milani G, Lourenço PB, Tralli A (2006a). Homogenised limit analysis of masonry walls. Part I: failure surfaces. Computers and Structures; 84: 166-180.

[35] Milani G, Lourenço PB, Tralli A (2006b). Homogenised limit analysis of masonry walls. Part II: structural examples. Computers and Structures; 84: 181-195.

[36] Milani G, Lourenço PB, Tralli A (2006c). Homogenization approach for the limit analysis of out-of-plane loaded masonry walls. Journal of Structural Engineering ASCE; 132 (10): 1650-1663.

[37] Milani E, Milani G, Tralli A (2008). Limit analysis of masonry vaults by means of curved shell finite elements and homogenization. International Journal of Solids and Structures; 45(20): 5258-5288.

[38] Munro J, Da Fonseca AMA (1978). Yield-line method by finite elements and linear programming. J. Struct. Eng. ASCE; 56B: 37-44.

[39] Orduna A, Lourenço PB (2005). Three-dimensional limit analysis of rigid blocks assemblages. Part I: Torsion failure on frictional interfaces and limit analysis formulation. International Journal of Solids and Structures; 42(18-19): 5140-5160.

[40] Sinha BP (1978). A simplified ultimate load analysis of laterally loaded model orthotropic brickwork panels of low tensile strength. Journal of Structural Engineering ASCE; 56B(4): 81-84.

[41] Southcombe C, May IM, Chong VL (1995). The behaviour of brickwork panels with openings under lateral load. Proc. 4th Int. Masonry Conf. Proc. Brit. Mas. Soc., London, UK, 1, 105-110.

[42] Strand 7.2 (2004).Theoretical Manual. www.strand7.com Sydney Australia; 1-410.

[43] Suquet P. Analyse limite et et homogeneisation (1983). Comptes Rendus de l'Academie des Sciences - Series IIB – Mechanics; 296: 1355-1358.

[44] Tamuzh VP (1962). On a minimum principle in dynamics of rigid-plastic bodies. Prikl. Math. Mek.; 26: 1067.

[45] Wang M, Hao H, Ding Y, Li ZX (2009). Prediction of fragment size and ejection distance of masonry wall under blast load using homogenized masonry material properties. International Journal of Impact Engineering, in press.

[46] Wu C, Hao H (2006). Derivation of 3D masonry properties using numerical homogenization technique. International Journal for Numerical Methods in Engineering; 66: 1717-1737.

[47] Wu C, Hao H (2008). Numerical derivation of averaged material properties of hollow concrete block masonry. Engineering Structures; 30: 870-883.

8 Figures
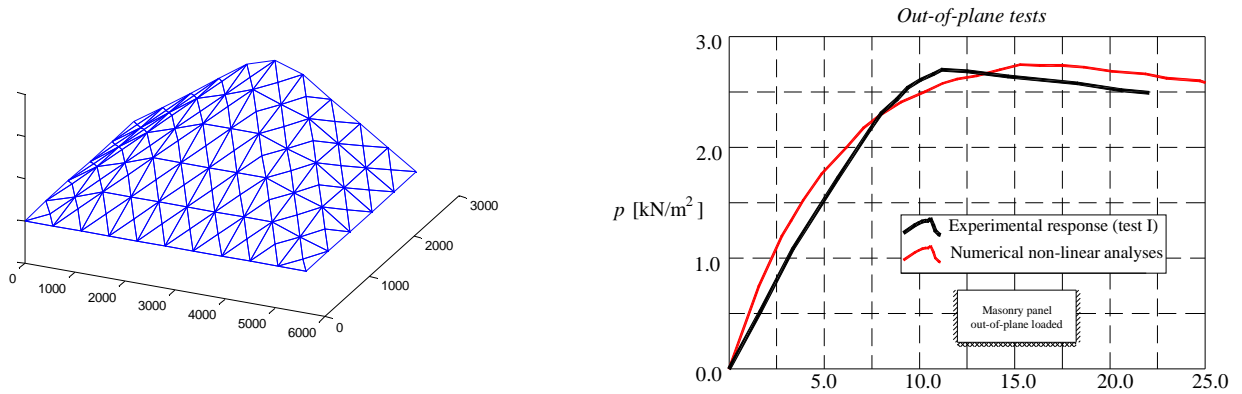
Figure 1: Typical relatively ductile behavior of a masonry wall in two-way bending and out-of-plane loaded (data from Southcombe et al. 1995, numerical simulations from Milani et al. 2006c).
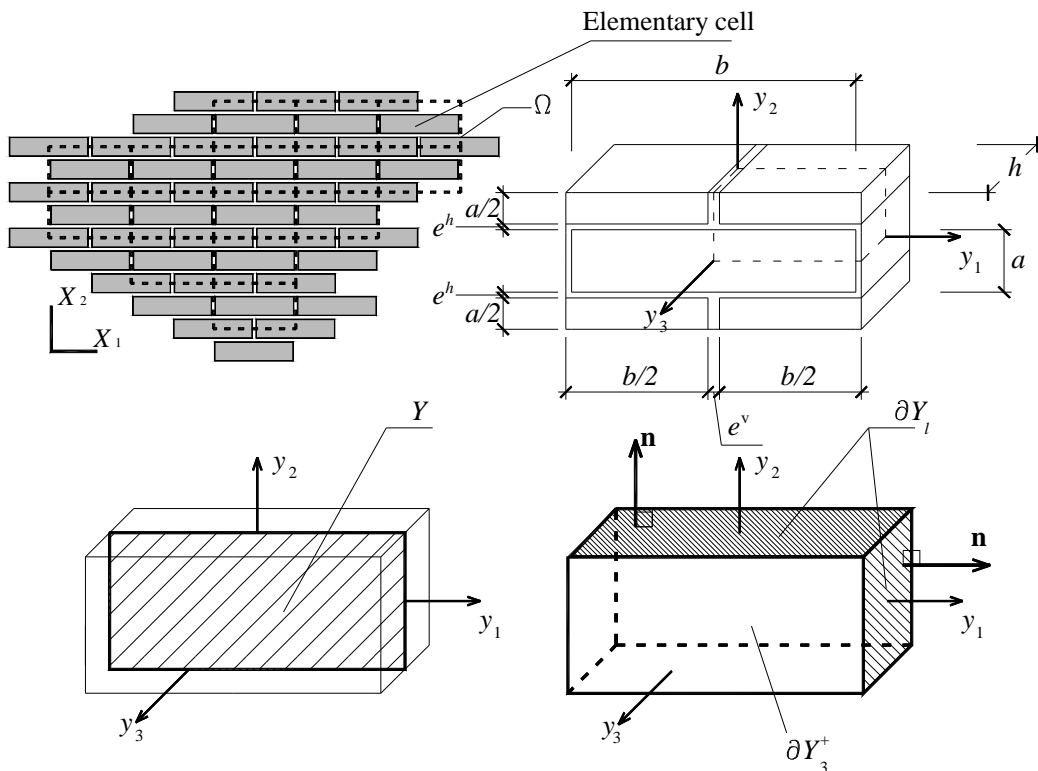
Figure 2: Periodic structure ($X_1 - X_2$: macroscopic frame of reference) and elementary cell ($y_1 - y_2 - y_3$: local frame of reference).

subdivision of masonry thickness in *layers*

$\Delta_{L\,i} = h/n_i$ known values

subdivision of each layer in 36 *sub-domains*

Bricks, joints and brick-joint interfaces strength domains

Brick-joints interfaces

Bricks and joints sub-domains

-a

-b

-c
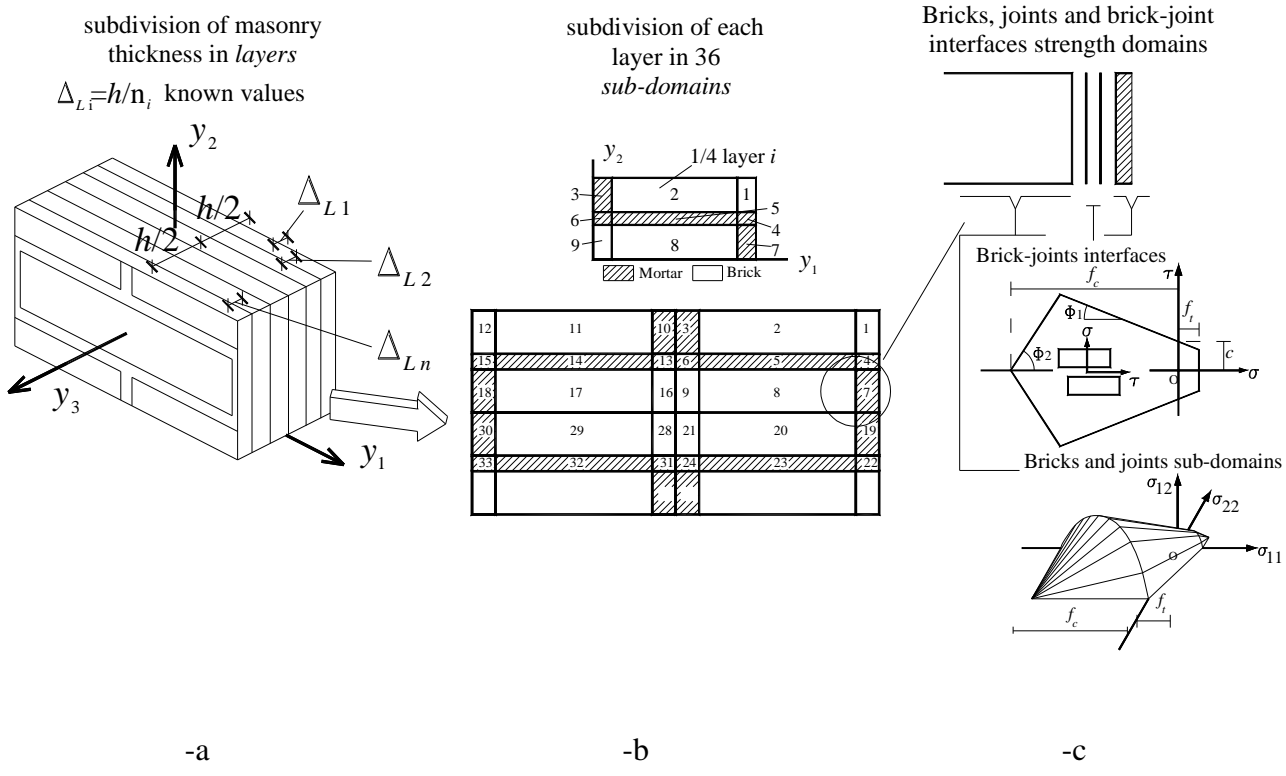
Figure 3: The micro-mechanical model proposed. -a: subdivision in layers along the thickness. –b: subdivision of each layer in sub-domains. –c: linearized strength domain for bricks and joints sub-domains, with Mohr-Coulomb failure criteria, and for bricks-joints interfaces, with a Mohr-Coulomb failure criterion with compression linearized cap and tension cutoff.
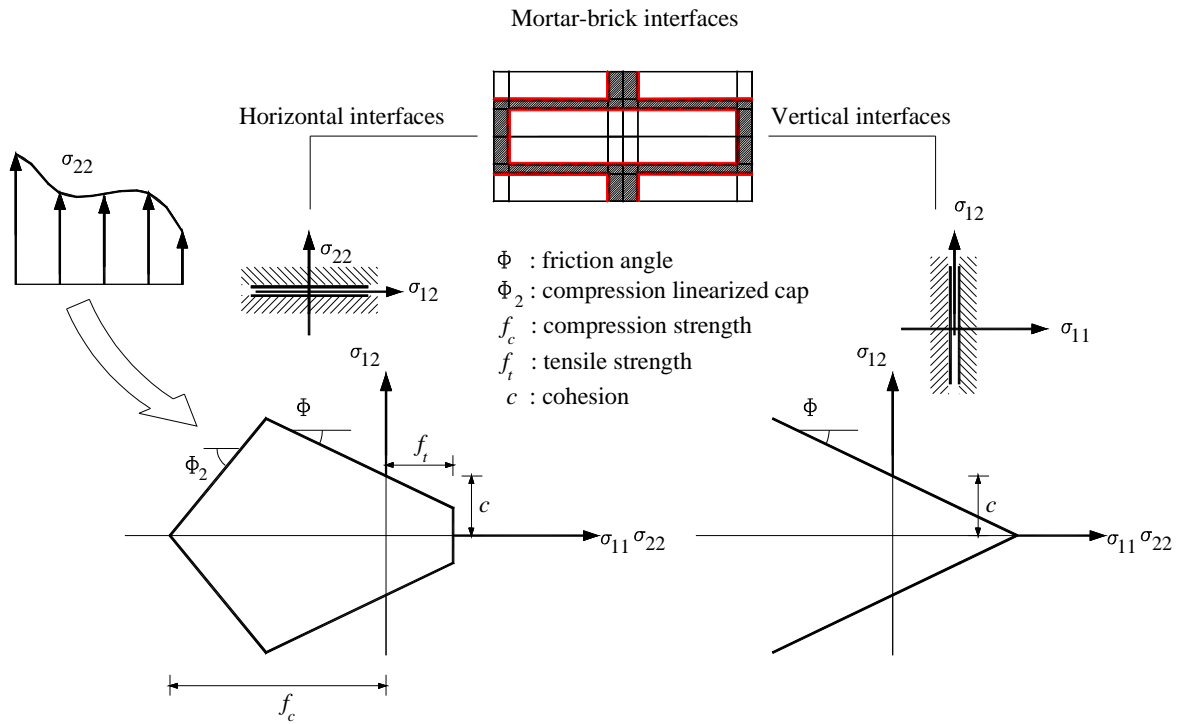
Mohr Coulomb with compression cap and
tension cut off failure criterion.

Classic Mohr Coulomb failure criterion.

-a

-b

Figure 4: Piecewise linear approximation of the failure criterion adopted for mortar-bricks
interfaces. -a: Mohr-Coulomb failure criterion with tension cut-off and linearized compression
cap. –b: classic Mohr-Coulomb failure criterion.
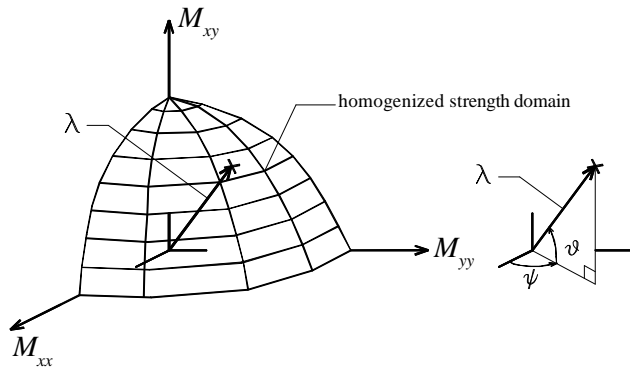
Figure 5: Meaning of λ multiplier in the optimization problem and ψ and ϑ angles.

-a   -b   -c
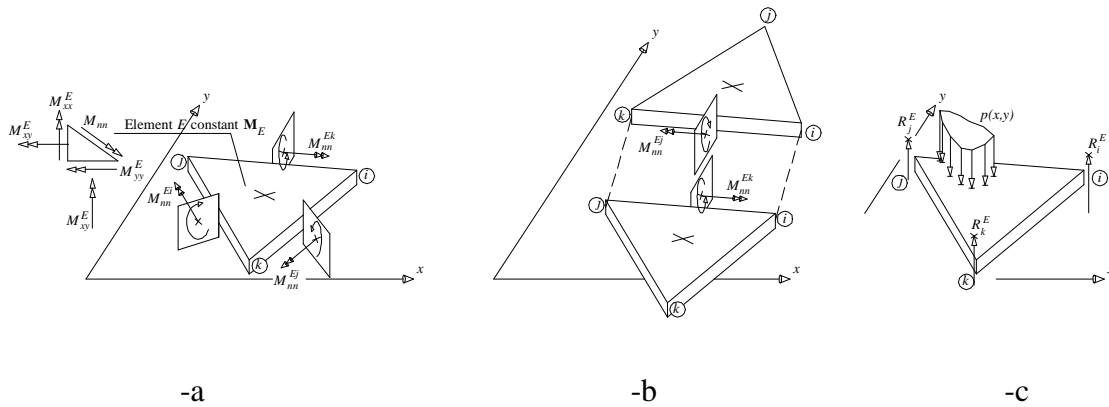
Figure 6: Bending moment acting at the edges of the triangular plate element used for the FE rigid-plastic analysis (-a), continuity of the bending moment on interfaces (-b), integral equilibrium (-c).

-a   -b   -c
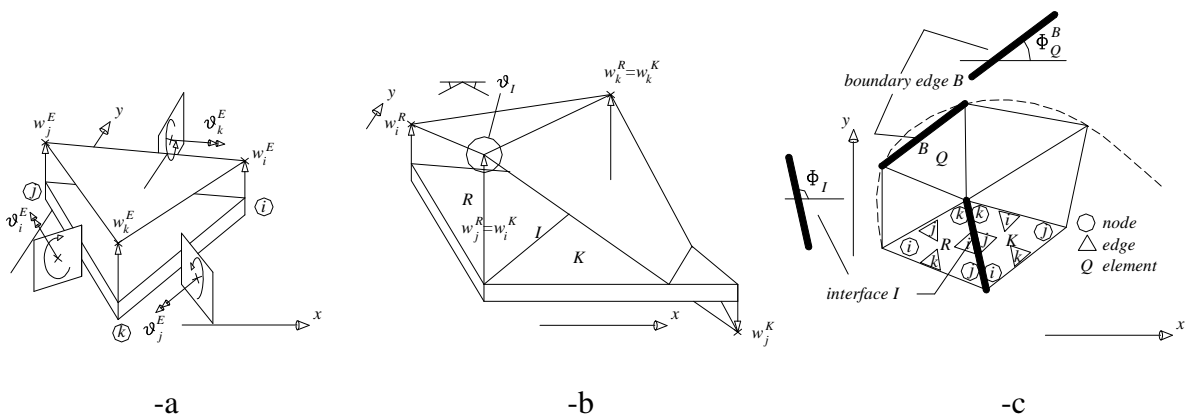
Figure 7: Rotations at the edges of the triangular plate element used for the FE rigid-plastic analysis (-a), mutual rotation along an interface between adjacent triangles (-b), discretization of the 2D domain (-c).
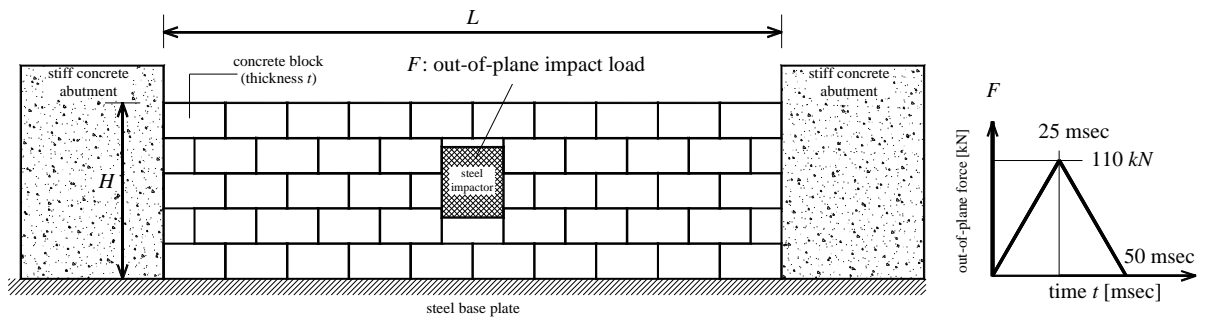
Figure 8: Stretcher bond masonry parapet subject to low velocity impact. Geometry of the wall and typology of dynamic load applied.
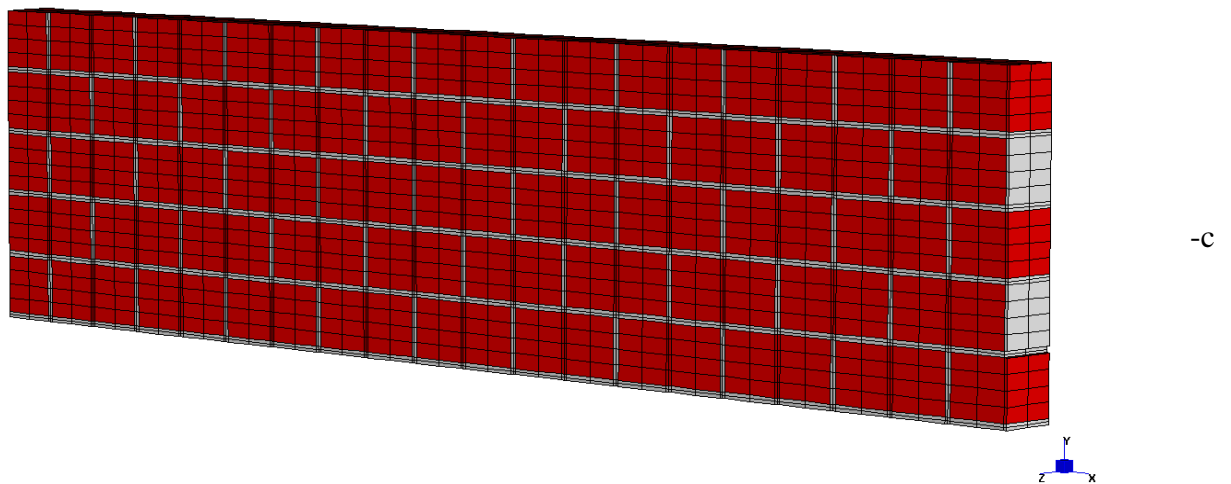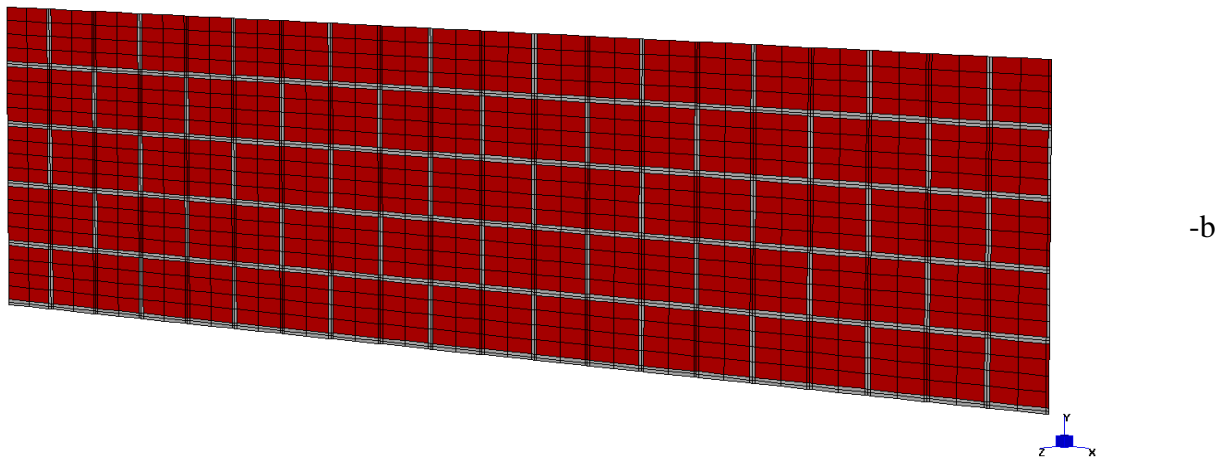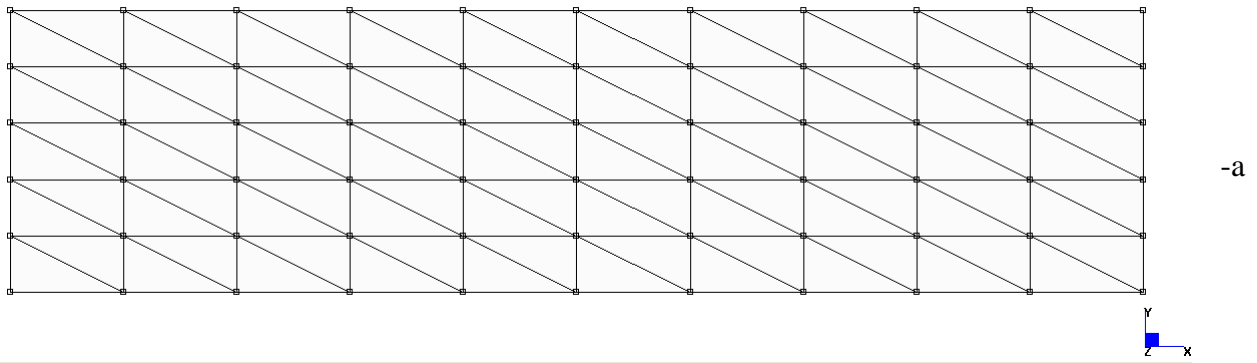
Figure 9: Stretcher bond masonry parapet subject to low velocity impact.–a: FE limit analysis discretization. –b: elastic-plastic 2.5D model discretization (WI2.5D). –c: elastic-plastic 3D model discretization (WI3D). Only ½ of the wall is analyzed for symmetry.
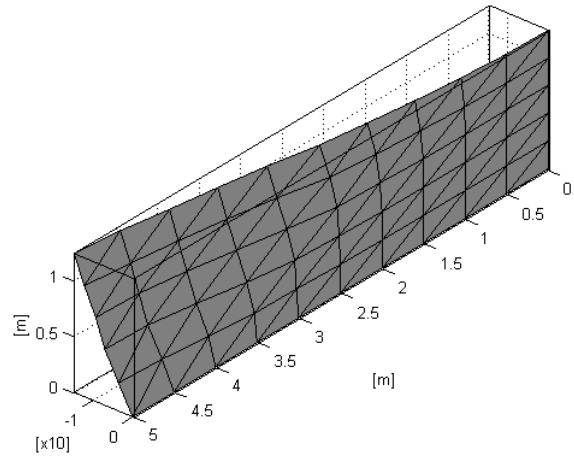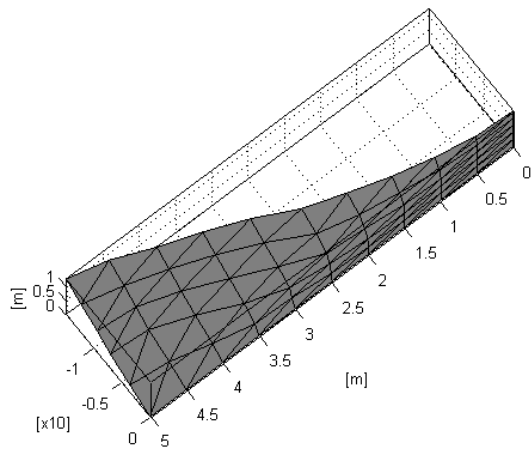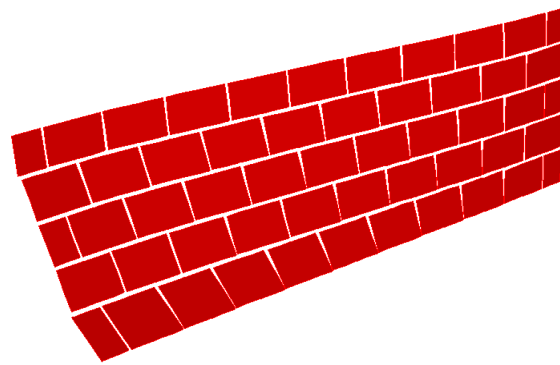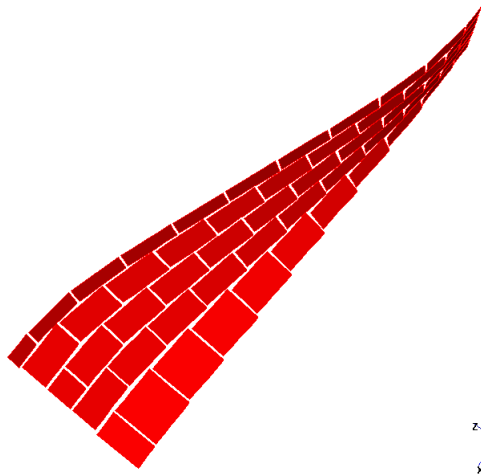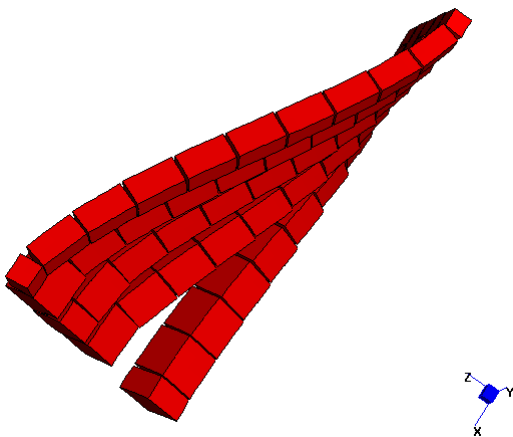
Figure 10: Stretcher bond masonry parapet subject to low velocity impact. Comparison among deformed shapes at t=100 msec –a: Homogenized limit analysis approach. –b: heterogeneous 2.5D elastic-plastic FE approach. –c: heterogeneous 3D elastic-plastic FE approach. Only ½ of the wall is analyzed due to symmetry.
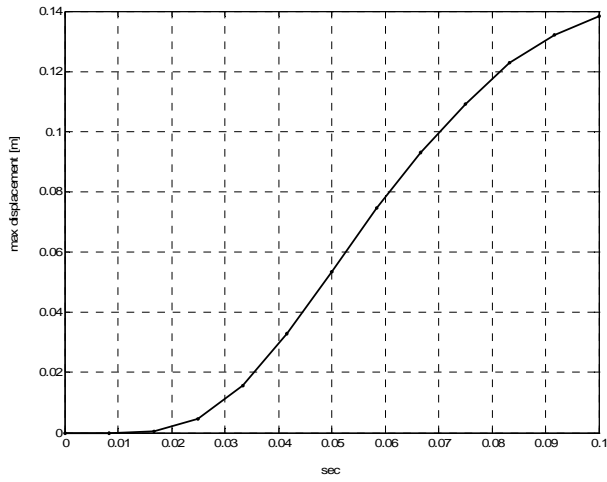
-a
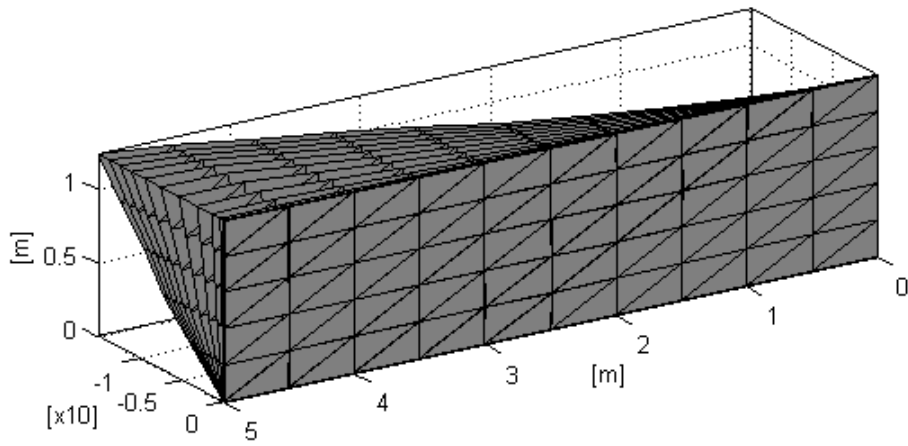
-b

Figure 11: Stretcher bond masonry parapet subject to low velocity impact. Results from the rigid-plastic model, CASE A. –a: maximum displacement-time diagram. –b: perspective view of deformed shape evolution.
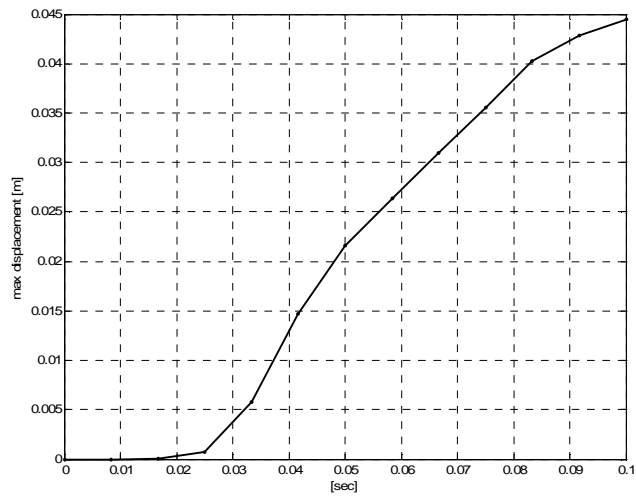
-a
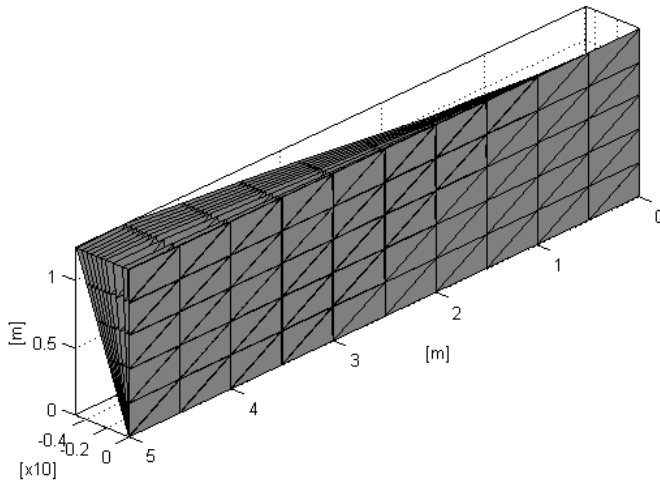
-b

Figure 12: Stretcher bond masonry parapet subject to low velocity impact. Results from the rigid-plastic model, CASE B. –a: maximum displacement-time diagram. –b: perspective view of deformed shape evolution.
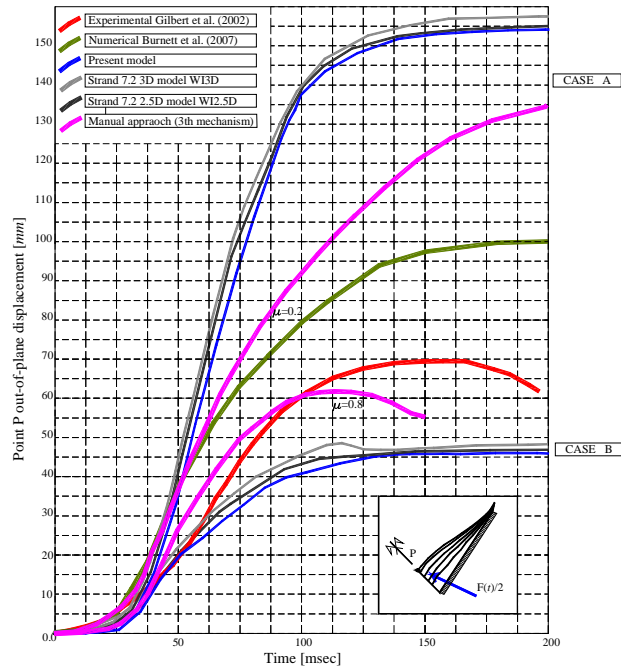
Figure 13: Stretcher bond masonry parapet subject to low velocity impact. Overview of time-maximum out-of-plane displacement diagrams.
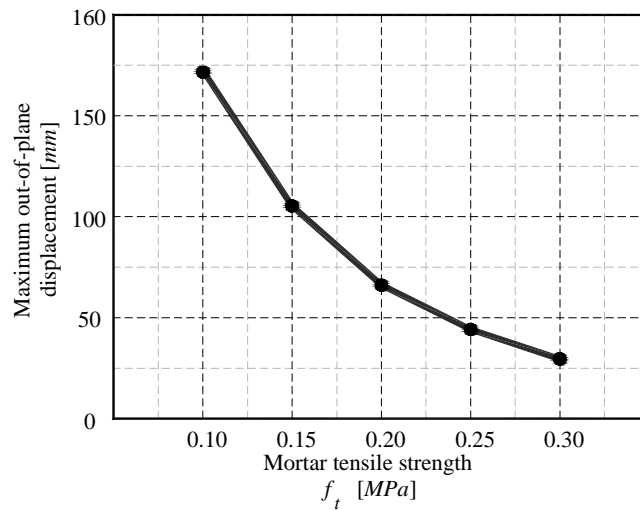
Figure 14: Maximum out-of-plane displacement (at the end of the simulations, 200 msec) at increasing mortar tensile strength.
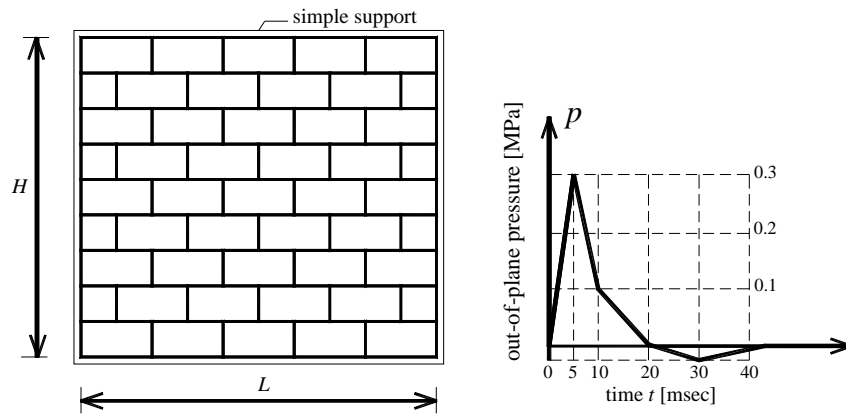
Figure 15: Masonry panel constrained at four edges and subjected to air-blast load.
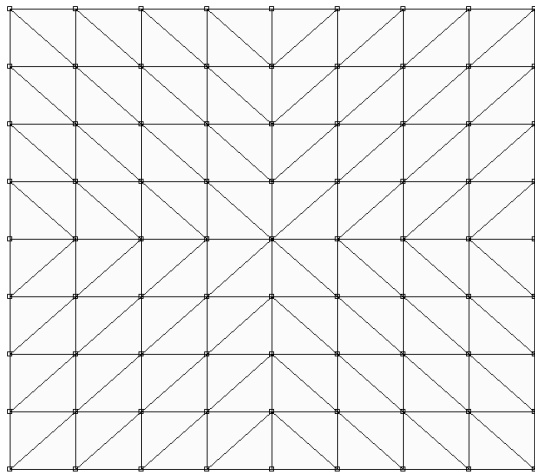
-a
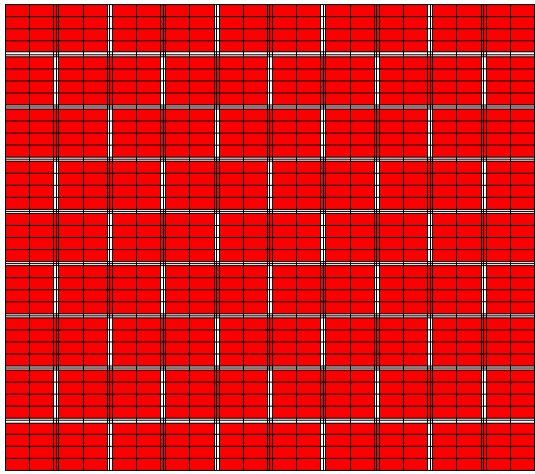
-b
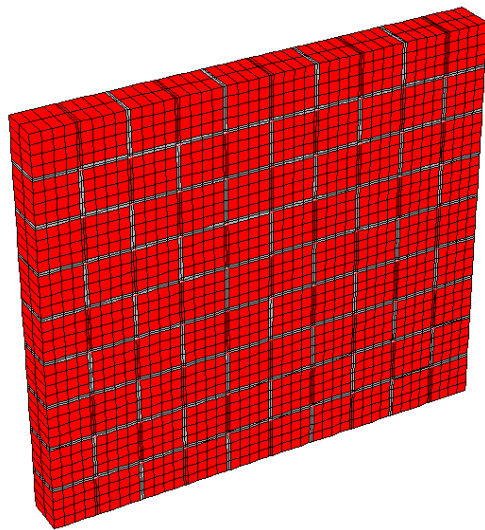
-c

Figure 16: Masonry panel constrained at four edges and subjected to air-blast load.–a: FE limit analysis discretization. –b: elastic-plastic 2.5D model discretization (WII2.5D). –c: elastic-plastic 3D model discretization (WII3D).
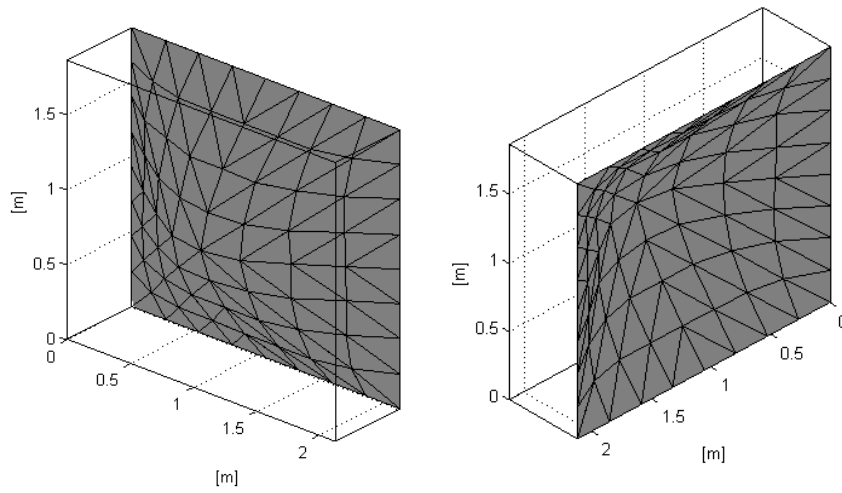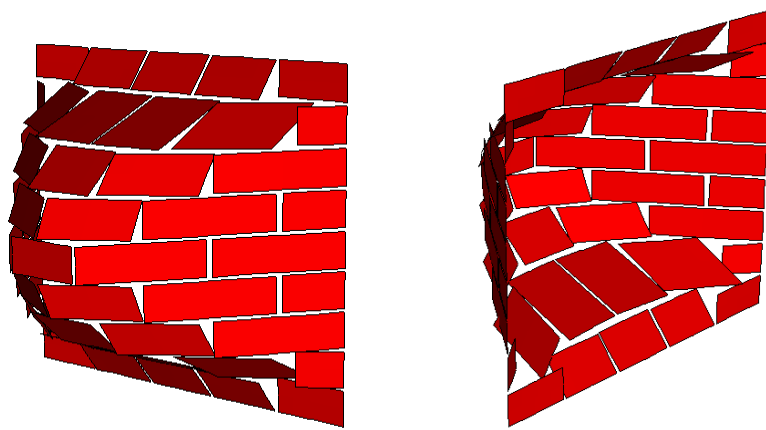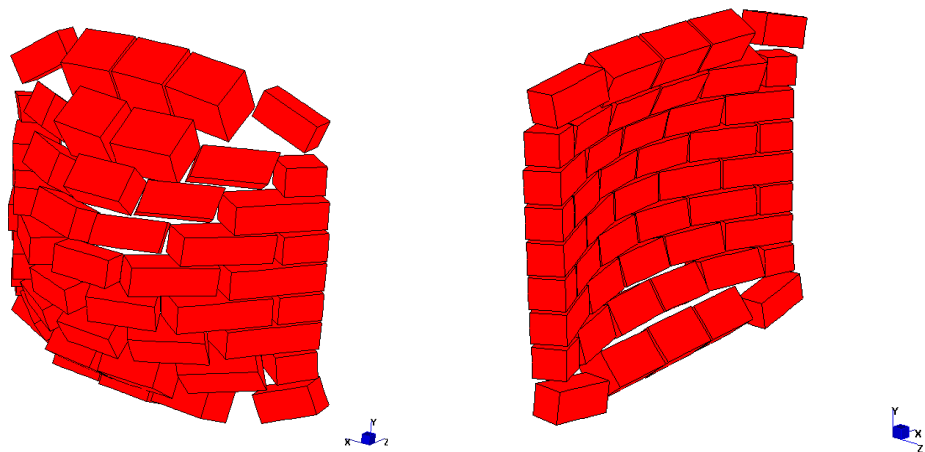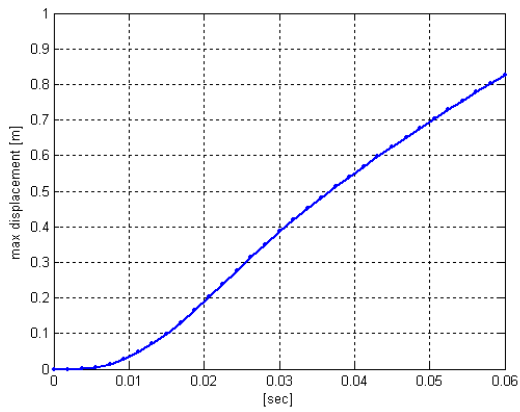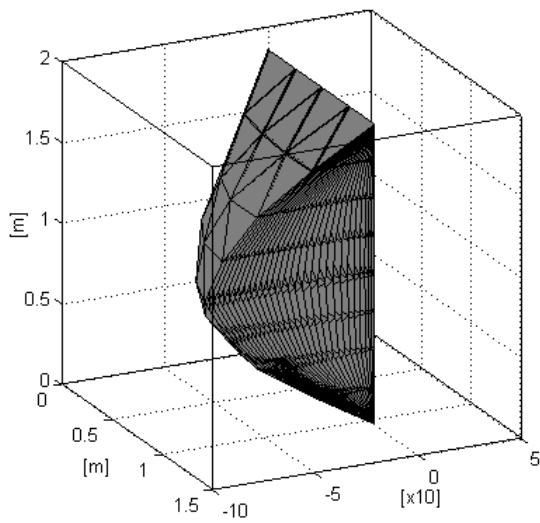
Figure 17: Masonry panel constrained at four edges. Comparison among deformed shapes at t=10 msec –a: Homogenized limit analysis approach. –b: heterogeneous 2.5D elastic-plastic FE approach. –c: heterogeneous 3D elastic-plastic FE approach.
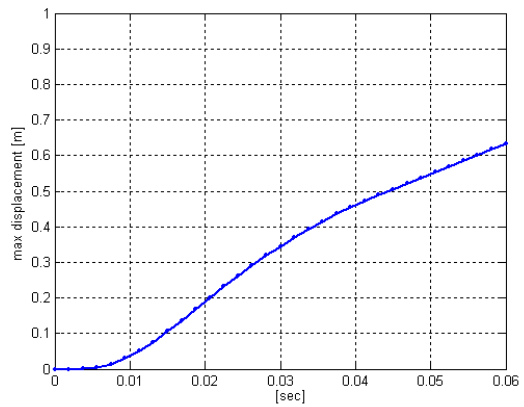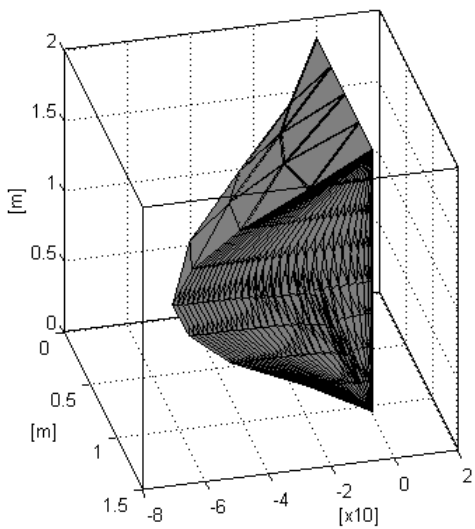
-a

-b

Figure 18: Masonry panel constrained at four edges and subjected to air-blast load, CASE A. –a: maximum displacement-time diagram. –b: perspective view of deformed shape evolution (1/2 of plate)

-a

-b

Figure 19: Masonry panel constrained at four edges and subjected to air-blast load, CASE B. –a: maximum displacement-time diagram. –b: perspective view of deformed shape evolution (1/2 of plate)
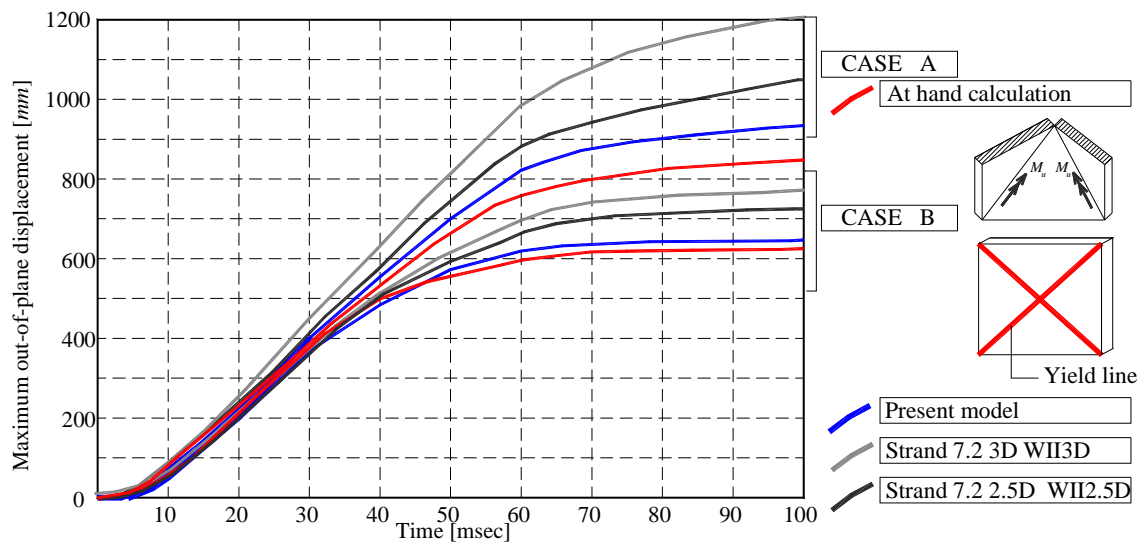
Figure 20: Masonry panel constrained at four edges and subjected to air-blast load. Time-maximum out-of-plane displacement diagrams.

9 Tables

Table I: Stretcher bond masonry parapet subject to low velocity impact. Mechanical characteristics assumed for bricks-mortar joints (f_t: tension cut-off, c: cohesion, Φ: friction angle, f_c: compressive strength, Φ_2: shape of the linearized compressive cap).

	f_t MPa	c	Φ	f_c MPa	Φ_2
CASE A	0.10	1.2 f_t	30°	20 f_t	30°
CASE B	0.25	1.2 f_t	30°	20 f_t	30°

Table II: Masonry panel constrained at four edges and subjected to air-blast load. Mechanical characteristics assumed for brick-mortar interfaces (f_t:tension cut-off, c: cohesion, Φ: friction angle, f_c: compressive strength, Φ_2: shape of the linearized compressive cap).

	f_t MPa	$c\left[\dfrac{N}{mm^2}\right]$	Φ	f_c MPa	Φ_2
CASE A	0.2	1.2 f_t	30°	5	30°
CASE B	0.5	1.2 f_t	30°	5	30°

	CASE	CPU time [h:m:sec]			Maximum displacement [mm]		
		Homogenized rigid-plastic	2.5D FEM	3D FEM	Homogenized rigid-plastic	2.5D FEM	3D FEM
Example 1	A	0:4:12	9:11:01	17:45:21	145 [1]	152 [1]	174 [1]
	B	0:3:56	12:27:44	21:09:51	46.2 [1]	47 [1]	48 [1]
Example 2	A	0:3:23	10:11:01	19:54:00	930 [2]	1050 [2]	1200 [2]
	B	0:2:49	11:38:19	20:51:47	650 [2] 625 [3]	720 [2]	770 [2]

Table III: CPU time required for the simulations and maximum displacement at the end of the simulations. Comparison between present numerical approach and standard FE heterogeneous procedures.

Legend

[1] maximum displacement calculated at 200 msec

[2] maximum displacement calculated at 100 msec

[3] at hand calculation based on the yield line theory